Regionalization of Present-Day Precipitation in the Greater Monsoon Region of Asia*

JESSICA L. CONROY

Department of Geosciences, The University of Arizona, Tucson, Arizona

JONATHAN T. OVERPECK

Department of Geosciences, Department of Atmospheric Sciences, and Institute of the Environment, The University of Arizona, Tucson, Arizona

(Manuscript received 26 August 2010, in final form 2 February 2011)

ABSTRACT

The spatial domain of the Asian monsoon has been defined by the intensity, seasonal concentration, and annual range of precipitation. Monsoon subdomains, such as the Indian monsoon, East Asian monsoon, and western North Pacific monsoon, have also been identified based on seasonal wind reversals as well as the timing and source of monsoon moisture. However, precipitation across the Asian monsoon region is heterogeneous and spatially complex and may have influences farther north than commonly assumed, particularly if scientists consider records of past variability spanning the current interglacial period. This paper presents an additional means of identifying the Asian monsoon domain and monsoon subsystems using an empirical orthogonal function (EOF)-based regionalization of gridded precipitation values. Regions of unique precipitation variability for the Asian monsoon region are determined using monthly precipitation anomalies from the Climate Prediction Center Merged Analysis of Precipitation (CMAP) gridded precipitation dataset from 1979 to 2009. From these regions, an area of Asian monsoon influence extending from the Arabian Sea eastward to the western North Pacific Ocean is defined, similar to other studies. One key difference is that this region of monsoon influence penetrates farther north into the Tibetan Plateau and northern China. Thus, paleoclimate observations of wetter conditions in these northern arid regions may suggest an intensification of monsoon moisture, rather than a northward shift in the boundary of the monsoon. In contrast, the Arabian Peninsula, largely removed from monsoon precipitation today, likely saw a shift of monsoon influence inland earlier in the Holocene. Also identified are different subdomains of distinct precipitation variability in southeastern Asia, the western North Pacific, and the East Asian monsoon region of northeastern China that agree with previous studies. Not identified in the paper is a single Indian summer monsoon region. Instead, the Arabian Sea was found to have unique precipitation variability relative to the Indian subcontinent. Summers with enhanced precipitation over the Arabian Sea coincide with decreased summer precipitation in the western North Pacific. This relationship is likely a result of the El Niño–Southern Oscillation (ENSO)-induced development of the Philippine Sea anticyclone. Local and remote sea surface temperatures were generally found to covary with regional precipitation, but not all regions respond similarly to the remote climate variability associated with ENSO. There is some evidence that the EOF-defined regions were stable through the Holocene, although additional regionalization analyses of paleorecords and model simulations of past precipitation variability are needed to reconstruct past regions of coherent precipitation variability.

1. Introduction

Almost two-thirds of the global population lives under the influence of the seasonal rains associated with the Asian monsoon (Clift and Plumb 2008). In coming decades, an expanded human population in the Asian monsoon region will depend on seasonal rainfall that is expected to vary significantly with increasing atmospheric greenhouse gas

* Supplemental information related to this paper is available at the Journals Online Web site: http://dx.doi.org/10.1175/2011JCLI4033.s1.

Corresponding author address: Jessica L. Conroy, Department of Geosciences, The University of Arizona, 1040 E. 4th St., Tucson, AZ 85721.
E-mail: jconroy@email.arizona.edu

DOI: 10.1175/2011JCLI4033.1

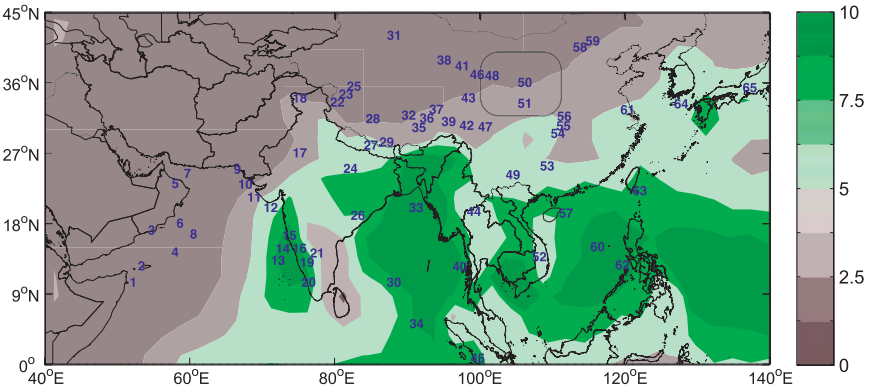

FIG. 1. Mean summer (JJAS) CMAP precipitation (mm day^{-1}) for 1979–2009 and locations of select paleoclimatic records of Asian monsoon variability. The ''box'' north and east of the figure center encompasses region of numerous loess records (#50 in Table 1).

concentrations (Annamalai et al. 2007; Turner et al. 2007; S. M. Lee et al. 2008; Ashfaq et al. 2009). Thus, improving predictability of monsoon rains is essential for effective planning and alleviation of future hydrologic stress within this densely inhabited region (Webster et al. 1998). However, projections of future Asian monsoon precipitation vary from model to model, and many models do not correctly simulate regional precipitation, evaporation, sea surface temperature (SST), and air–sea interactions (Bollasina and Nigam 2009). Asian monsoon predictability and accurate projections of the future Asian monsoon require an understanding of the oceanic and atmospheric processes of the monsoon system, the influence of atmospheric and oceanic teleconnections, and the spatial and temporal variability of rainfall on intraseasonal, interannual, multidecadal, and longer time scales. However, the spatial heterogeneity of rainfall over the Asian monsoon region hampers predictive efforts because precipitation in this vast region does not necessarily covary or respond coherently to changes in forcing factors (Zhou et al. 2009).

Understanding regional monsoon behavior on interdecadal-to-millennial time scales is also key and must be informed by paleoclimatic observations. Thus, it is critical to know if paleoclimate reconstructions of Asian monsoon variability from diverse regions, such as ocean sediment cores from the Arabian Sea (Overpeck et al. 1996; Clemens and Prell 2003; Gupta et al. 2008), lake sediment records from the Tibetan Plateau (Wei and Gasse 1999; Morrill et al. 2006; Mügler et al. 2010), and speleothem records from across China (Y. J. Wang et al. 2001; Wang et al. 2005; Y. J. Wang et al. 2008), should be expected to covary with one another as a function of variability time scale and climate forcing (Fig. 1; Table 1). For example, there is disagreement between Asian monsoon proxies from Arabian Sea sediments and speleothems from southern China about the timing of maximum monsoon intensity during the early Holocene period (Ruddiman 2006; Clemens and Prell 2007). Another point of contention is why some paleoprecipitation records indicate abrupt changes in monsoon intensity in the mid-Holocene (Morrill et al. 2003), whereas others suggest more gradual changes less prone to threshold behavior (Fleitmann et al. 2007). We hypothesize that some of these discrepancies between precipitation reconstructions may be due to the location of paleorecords in regions that experience different precipitation regimes.

It has been recognized by many researchers that the East Asian and Indian monsoons are independent systems (B. Wang et al. 2001; Ding and Chan 2005; Huang et al. 2007). The East Asian monsoon region has been further divided into several subsystems, including the East Asian summer monsoon and western North Pacific (WNP) summer monsoon (B. Wang et al. 2001; Wang and LinHo 2002). These subregions are defined by the source, timing, and location of seasonal precipitation and are represented by atmospheric indices that reflect regional precipitation variability (Wang and Fan 1999; B. Wang et al. 2001, 2008). Empirical orthogonal function (EOF)-based regionalization offers an additional way of dividing a large area into coherent subregions with similar variability (White et al. 1991). Previous regionalization studies within the Asian monsoon region have been limited to irregularly spaced station data from individual countries, such as Nepal, China, and India, and have not considered the entire region of Asian monsoon influence (Iyengar and Basak 1994; Singh and Singh 1996; Gadgil 2003; Kansakar et al. 2004; Lu et al. 2008). Other studies have been larger in scope, performing EOF analysis on global-scale datasets to understand the global monsoon system (Trenberth et al. 2000; Zhang and Wang 2008). In this paper, we use EOF analysis on a broader, more spatially complete, gridded

precipitation product to define both the region of Asian monsoon influence and subregions with unique precipitation variability. We support our results from this approach by applying the same EOF-based regionalization to two additional precipitation products. We also assess the relationship between precipitation time series of the different regions and various spatiotemporal aspects of monsoon climate to understand the large-scale atmospheric processes driving precipitation variability in each of the regions. Lastly, we highlight the implications for paleoclimatic observations of Asian monsoon variability based on our definition of precipitation domains and our understanding of the atmospheric dynamics and teleconnections associated with each region.

2. Data

We evaluated three gridded precipitation products over the Asian monsoon region (defined as 0°–45°N, 40°–140°E): the Climate Prediction Center Merged Analysis of Precipitation (CMAP) enhanced dataset, the Global Precipitation Climatology Project (GPCP) dataset, and the Tropical Rainfall Measuring Mission (TRMM) 3B43 dataset (Xie and Arkin 1997; Kummerow et al. 1998; Adler et al. 2003). We used gridded datasets because they provide regularly spaced, quality-controlled estimates of precipitation; EOF analysis on irregularly spaced station data may affect loading patterns (Karl et al. 1982). CMAP precipitation is a merged composite of precipitation estimates from satellite data, available station data, and National Centers for Environmental Prediction (NCEP) reanalysis data (Xie and Arkin 1997). GPCP precipitation is also a merged composite of satellite estimates of precipitation and station data (Adler et al. 2003). The CMAP and GPCP datasets contain monthly precipitation data in millimeters per day and have a 2.5° × 2.5° spatial resolution, giving us 720 grid points in our defined Asian monsoon region. Monthly CMAP data extend from January 1979 to September 2009, and monthly GPCP data extend from January 1979 to July 2009 (Xie and Arkin 1997; Adler et al. 2003). TRMM precipitation is a composite of the high-resolution TRMM satellite precipitation estimates combined with gridded, quality-controlled station data from 50°S to 50°N (Kummerow et al. 1998). The TRMM dataset contains precipitation rate data in millimeters per hour, has a 0.25° × 0.25° spatial resolution, and extends from January 1998 to December 2009. We averaged the TRMM grid points together, creating a 1° × 1° gridded dataset (4500 grid points) to reduce computational time. Since the gridded precipitation data are highly nonnormal, with many zero values in the more arid regions, we took the square root of each monthly precipitation estimate, which produced more normally distributed data (Comrie and Glenn 1998). Sea level pressure (SLP) and 850-mb wind data used in this analysis are from the NCEP–Department of Energy Global Reanalysis 2 (NCEP-2) (Kanamitsu et al. 2002), and SST data are from the Met Office Hadley Centre Sea Ice and Sea Surface Temperature, version 1.1 (HadISST1.1), dataset (Rayner et al. 2003).

3. Methods

We performed EOF analysis on the gridded monthly precipitation anomalies for each of the three datasets using MATLAB, decomposing the time–space precipitation matrices into their eigenvectors and associated eigenvalues to find regions with covarying precipitation anomalies. We did not remove the seasonal cycle because we are interested in grouping grid points with similar precipitation seasonality. In fact, the power of the annual cycle may be one of the defining factors of regional precipitation regimes. We chose to perform EOF analyses on the correlation matrices, rather than the covariance matrices, because we are considering regions with widely varying precipitation amounts and wish to delimit regions of precipitation variability based on similar seasonal patterns and associated atmospheric mechanisms, rather than the total amount of variance. To determine the number of significant eigenvalues and associated eigenvectors, we employed the Rule N test, the North test, and the scree test on the eigenvalues of each precipitation dataset (Cattell 1966; North et al. 1982; Overland and Preisendorfer 1982). For the Rule N test, we generated 1000 random matrices with the same size, variance, mean annual cycle, and first-order autoregression (AR1) coefficients as the CMAP, GPCP, and TRMM datasets. We decomposed each of these datasets, sorted the resulting eigenvalue variances, and selected the 99th percentile as our cutoff for eigenvalue significance. We calculated the distance between adjacent eigenvalues and the sampling error for each eigenvalue for the North test. Significant eigenvalues were those in which the distance between adjacent eigenvalues exceeded the error. The scree test was based on a visual inspection of slope change between adjacent eigenvalues. Once we selected the number of significant eigenvalues with these criteria, we rotated the retained eigenvectors using Promax oblique rotation with $k = 2$ (Hendrickson and White 1964). Rotation of eigenvectors is required in regionalization schemes to deal with several problems, including Buell patterns, or domain-shape dependence, of the loading patterns (Buell 1979). White et al. (1991) found that oblique rotations produced more stable loading patterns than unrotated or orthogonally rotated eigenvectors.

TABLE 1. List of paleoclimate records influenced by the Asian monsoon, plotted in Fig. 1.

No. on map	Lat (°N)	Lon (°E)	Proxy archive	Site	Select references
1	10.5	51.6	Ocean sediment	Northwest Arabian Sea	Zonneveld et al. (1997)
2	12.6	52.7	Speleothem	Dimarshim Cave	Fleitmann et al. (2007)
3	17.1	54.1	Speleothem	Defore Cave, Qunf Cave	Fleitmann et al. (2007)
4	14.3	57.3	Ocean sediment	Northwest Arabian Sea	Sirocko et al. (1993)
5	23.1	57.4	Speleothem	Hoti Cave	Fleitmann et al. (2007)
6	18.0	58.0	Ocean sediment	Northwest Arabian Sea	Anderson et al. (2002); Gupta et al. (2003)
7	24.4	59.0	Ocean sediment	Gulf of Oman	Cullen et al. (2000)
8	16.6	59.9	Ocean sediment	Owen Ridge	Clemens and Prell (2003)
9	24.9	65.9	Ocean sediment	North Arabian Sea	Luckge et al. (2001)
10	23.0	66.5	Ocean sediment	North Arabian Sea	Staubwasser et al. (2003)
11	21.8	68.0	Ocean sediment	East Arabian Sea	Agnihotri et al. (2002)
12	20.0	70.0	Ocean sediment	Southeast Arabian Sea	Sarkar et al. (2000)
13	13.3	71.0	Ocean sediment	Southeast Arabian Sea	Prabhu et al. (2004)
14	15.0	71.7	Ocean sediment	Southeast Arabian Sea	Prabhu et al. (2004)
15	15.5	72.6	Ocean sediment	Southeast Arabian Sea	Van Campo (1986)
16	14.8	74.0	Ocean sediment	Southeast Arabian Sea	Caratini et al. (1994)
17	27.0	74.0	Lake sediment	Northwest Indian Lakes	Roy et al. (2006); Prasad and Enzel (2006)
18	34.0	74.0	Tree-ring records	Karakoram	Treydte et al. (2006)
19	13.0	75.0	Speleothem	Akalagavi Cave	Yadava and Ramesh (2006)
20	10.5	75.2	Ocean sediment	Southeast Arabian Sea	Van Campo (1986)
21	14.2	76.4	Lake sediment	Indian Tank	Shankar et al. (2006)
22	33.7	79.2	Lake sediment	Bangong Co	Gasse et al. (1996)
23	34.5	80.4	Lake sediment	Sumxi Co and Longmu Co	Gasse et al. (1991)
24	25.0	81.0	Speleothem	Sota Cave	Yadava and Ramesh (2006)
25	35.3	81.5	Ice core	Guliya	Thompson et al. (1997)
26	19.0	82.0	Speleothem	Dandak Cave	Sinha et al. (2007)
27	28.0	84.1	Speleothem	Siddha Baba Cave	Denniston et al. (2000)
28	31.4	84.1	Lake sediment	Zabuye Lake	Wang et al. (2002)
29	28.4	85.7	Ice core	Dasuopu	Thompson et al. (2000)
30	28.0	87.0	Ice core	Mount Everest	Kaspari et al. (2007)
31	42.0	87.0	Lake sediment	Bosten Lake	Wünnemann et al. (2006)
32	31.8	89.0	Lake sediment	Siling Co	Morinaga et al. (1993)
33	20.0	90.0	Ocean sediment	Bay of Bengal	Kudrass et al. (2001)
34	5.2	90.1	ocean sediment	Bay of Bengal	Ahmad et al. (2008)
35	30.7	90.4	Lake sediment	Nam Co	Mügler et al. (2010)
36	31.4	91.5	Lake sediment	Co Ngion	Shen et al. (2008a); Tang et al. (2009)
37	31.6	92.1	Lake sediment	Ahung Co	Morrill et al. (2006); Tang et al. (2009)
38	38.9	93.9	Lake sediment	Sugan Lake	Holmes et al. (2007)
39	31.0	94.5	Tree-ring records	Northeast Tibet	X. C. Wang et al. (2008)
40	12.5	96.0	Ocean sediment	Andaman Sea	Rashid et al. (2007)
41	38.1	96.4	Ice core	Dunde	Liu et al. (1998)
42	30.5	97.0	Tree-ring records	South Tibet	Bräuning and Mantwill (2004)
43	34.0	97.2	Lake sediment	Lake Koucha	Mischke et al. (2008)
44	19.5	98.0	Tree-ring records	Thailand	Buckley et al. (2007)
45	0.0	98.5	Coral	Mentawai Islands	Abram et al. (2007)
46	37.0	98.7	Tree-ring records	Northeast Tibet	Huang and Zhang (2007)
47	30.3	99.6	Lake sediment	Yidun Lake	Shen et al. (2008b)
48	36.9	100.3	Lake sediment	Lake Qinghai	Colman et al. (2007)
49	24.2	103.4	Speleothem	Xiaobailong Cave	Cai et al. (2006)
50	36.0	105.0	Loess	Many sections within box	Liu and Ding (1998); Herzschuh (2006);
51	33.3	105.0	Speleothem	Wangxiang Cave	Zhang et al. (2008)

TABLE 1. (*Continued*)

No. on map	Lat (°N)	Lon (°E)	Proxy archive	Site	Select references
52	13.7	107.0	Lake sediment	Ratanakiri Province	Maxwell (2001)
53	25.3	108.1	Speleothem	Dongge Cave	Yuan et al. (2004); Wang et al. (2005); Dykoski et al. (2005)
54	29.5	109.6	Speleothem	Lianhua Cave	Cosford et al. (2008)
55	30.5	110.3	Speleothem	Heshang Cave	Hu et al. (2008)
56	31.7	110.4	Speleothem	Sanbao Cave	Y. J. Wang et al. (2008)
57	19.3	110.7	Coral	South China Sea	Sun et al. (2005)
58	40.5	112.6	Lake sediment	Daihai Lake	Xiao et al. (2006)
59	41.3	114.3	Lake sediment	Anguli-nuur Lake	Wang et al. (2010)
60	15.0	115.0	Ocean sediment	South China Sea	Wang et al. (1999)
61	32.5	119.2	Speleothem	Hulu Cave	Y. J. Wang et al. (2001)
62	12.7	119.5	Ocean sediment	Sulu Sea	Wei et al. (2003)
63	22.2	120.8	Lake sediment	Dongyuan Lake	Lee and Liew (2010)
64	33.3	126.6	Lake sediment	Hanon paleo-maar	S. H. Lee et al. (2008)
65	35.3	136.0	Lake sediment	Lake Biwa	Ishiwatari et al. (2009)

We identified regions of unique precipitation variability using two methods. The first method is based on the maximum loading values. After decomposition and rotation, each grid point is represented by a set of loading values equal to the number of retained and rotated eigenvectors (e.g., Comrie and Glenn 1998). Each set of loading values can then be ranked by magnitude. For example, if the loading value for the leading EOF (EOF1) is higher than the loading values of the subsequent EOFs for a grid point, we incorporated that grid point into EOF region "1." Demarcation of the EOF regions in this manner produced coherent regions that mirror the areas of highest loading values for each EOF (Fig. S2, all supplemental figures and material can be accessed at http://dx.doi.org/10.1175/2011JCLI4033.s1). We also created composite plots of precipitation anomalies for months in the principal component (PC) time series with standard deviations $\geq|1.5|$. This method produced similar regions compared to the maximum loading method (Fig. S3). In the CMAP and GPCP datasets, 5% of the grid points in the plot of maximum loadings were out of place (8% in the TRMM dataset), with an isolated grid point from a remote region lying within a coherent region. In these few instances when an identified "region" contained a few isolated grid points from different regions, we imparted the isolated grid points with the region number of their second highest loading value to obtain more accurate regional precipitation averages. Most often in these cases, the second-highest loading value is the same as the maximum loading values of the surrounding grid points. After replacing these few grid points, the average precipitation time series calculated from all the grid points in a region is still highly correlated with the associated PC, providing support for our methodology.

4. Results

The Rule N test, North test, and scree tests indicate nine significant eigenvalues for the CMAP and GPCP datasets (Fig. S1). For the TRMM precipitation dataset, Rule N suggests only five significant eigenvalues, whereas the scree test suggests either five or nine significant eigenvalues, and the North test suggests nine significant eigenvalues. In some EOF-based studies that attempt to determine climate modes, only the top few eigenvalues are retained (e.g., those explaining more than ~5% of the total variance), as many of the higher-order eigenvalues are not physically interpretable (e.g., Quadrelli and Wallace 2004). However, we are using EOF analysis as a data reduction tool and wish to group a large number of grid points into a manageable set of regions with distinct temporal precipitation variability. Thus, we also require simple structure, or the delimitation of clear, coherent regions with high loading values (Richman 1986). The percent variance explained by our eigenvalues drops below 5% after the third eigenvalue in each dataset, but retaining only three eigenvalues results in poor simple structure; retaining more eigenvalues produces improved simple structure. Thus, we decided to follow the results of our three tests and retain nine eigenvalues and associated eigenvectors for the CMAP and GPCP datasets. There is some discrepancy between the eigenvalue retention tests for TRMM, but we decided to retain nine eigenvalues, as this resulted in improved simple structure compared to retaining only five eigenvalues. These eigenvalues explain 70.1%, 69.6%, and 64.9% of the total variance for the CMAP, GPCP, and TRMM datasets, respectively (Table 2). Although the percentage of variance explained by some of the higher-order eigenvalues

TABLE 2. Percent variance explained by the first nine unrotated and rotated eigenvalues of the CMAP, GPCP, and TRMM precipitation datasets.

Eigenvalue	CMAP unrotated	CMAP rotated	GPCP unrotated	GPCP rotated	TRMM unrotated	TRMM rotated
1	38.88	33.42	39.04	36.80	35.54	29.34
2	10.35	18.18	10.73	20.08	9.87	8.89
3	6.16	11.15	6.30	7.40	4.78	7.11
4	3.63	4.53	3.75	4.24	3.68	4.03
5	3.01	5.46	3.17	8.69	3.26	5.92
6	2.29	6.17	2.33	5.03	2.18	16.43
7	2.26	3.48	2.13	2.93	2.05	10.32
8	1.79	5.57	1.93	7.78	1.89	9.40
9	1.72	12.04	1.48	7.04	1.69	8.57

is fairly low, maps of eigenvector values indicate clear, coherent regions of high loading values for these higher-order EOFs (Fig. S2). In each dataset, one or two EOF loading patterns show a dipole-like structure, with one area having strong positive loading values and the other area having strong negative loading values (e.g., region 2 in CMAP and GPCP). White et al. (1991) suggest that ''splintering'' of regions indicates overfactoring, but retaining less than nine eigenvectors results in split regions as well. Split regions are designated by ''a'' and ''b'' in the regionalization maps.

The EOF number that defines the regions is often different in the three precipitation datasets, and there are differences in the sizes of regions. Yet, overall the regions are remarkably similar, providing additional confidence in our regionalization scheme (Fig. 2). The largest differences among the three datasets are the subdivision of the Arabian Sea and western North Pacific Ocean into three regions in the TRMM dataset. However, the TRMM dataset has much higher spatial resolution and far fewer months of data compared to the CMAP and GPCP datasets, which likely influences the results of the EOF analysis. The spatial differences between regions in CMAP and GPCP are small enough that because of the limits of space, we only analyze the results from the CMAP dataset in the following sections. Regions defined with the TRMM data vary more compared to the CMAP and GPCP results, but the much shorter length of the TRMM dataset precludes performing the same statistical analyses used on the CMAP regions in the following sections.

5. Discussion

a. Regional precipitation climatology

The PCs and time series of average monthly precipitation for each region are highly correlated, which is additional evidence that our criteria for region selection are sound (Fig. 3). Although the seasonal cycle is dominant in many of the time series, the monthly precipitation climatology for each region indicates differences in the seasonality of precipitation (Fig. 4). Regions 1, 2a, 3, 5, and 9 have a strong monsoonal signal, with peak precipitation occurring between May and September. More than 57% of the annual precipitation in these regions comes in the summer months [May–September (MJJAS)],

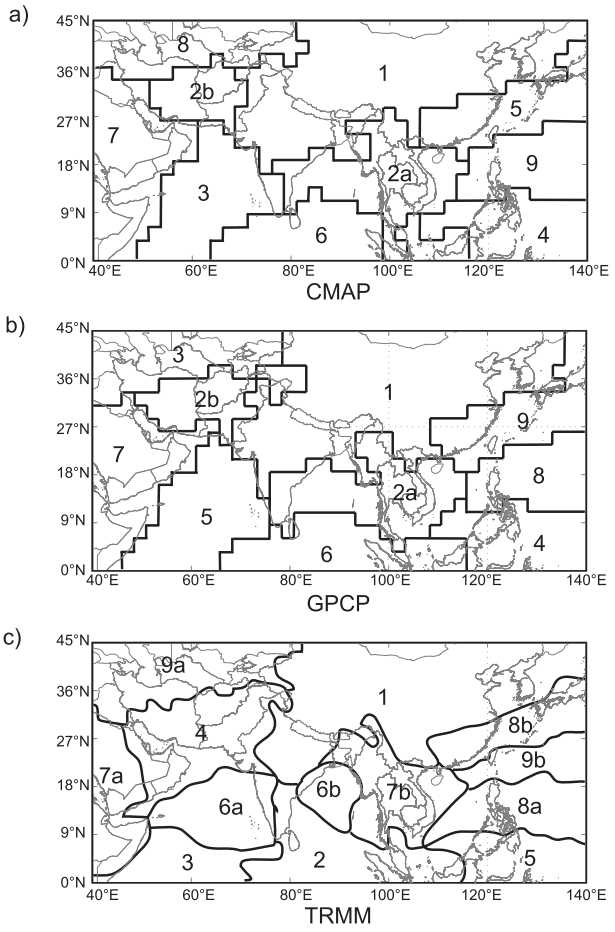

FIG. 2. Regions delimited by maximum loading values for the (a) CMAP, (b) GPCP, and (c) TRMM datasets.

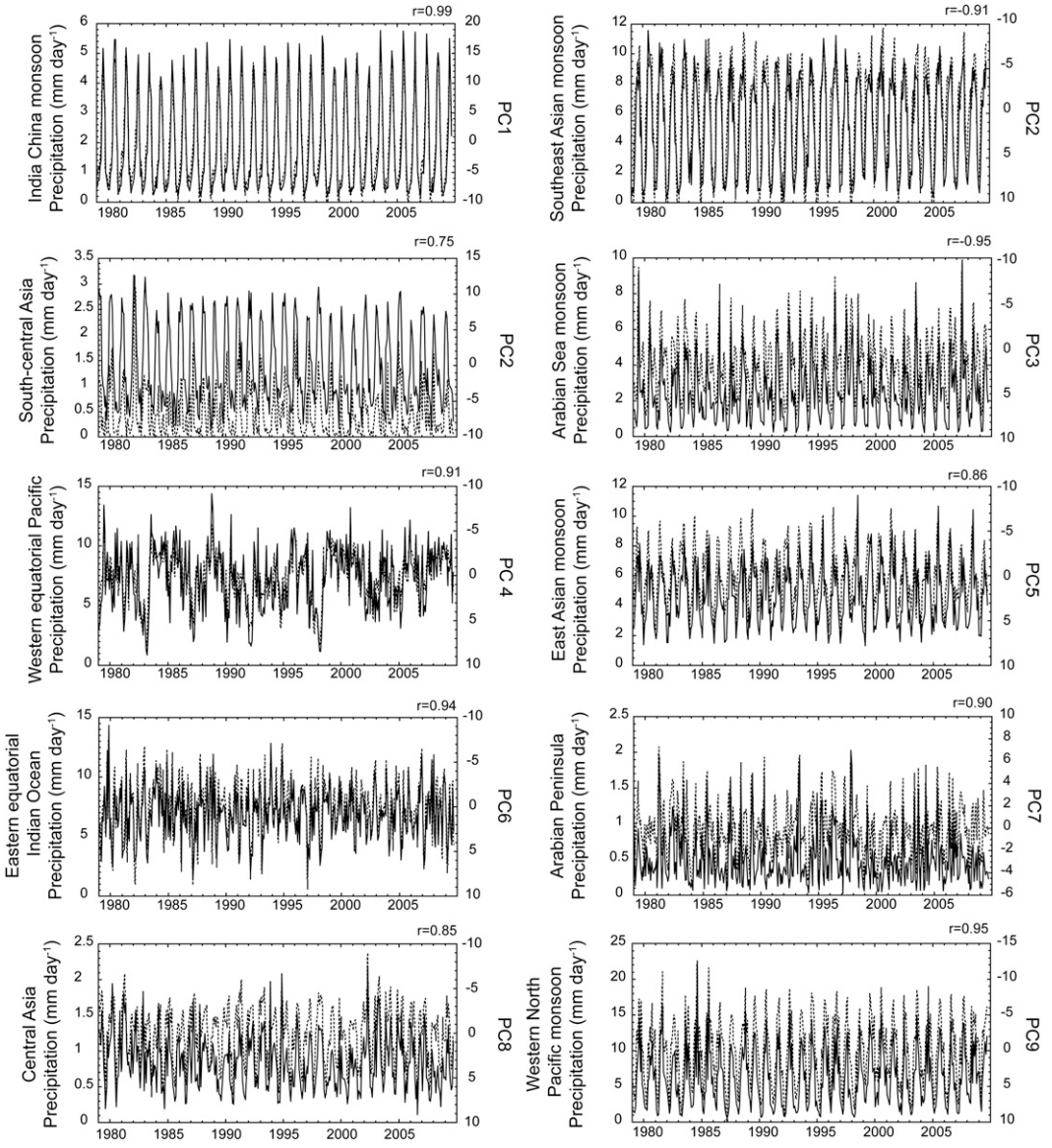

FIG. 3. Time series of precipitation averaged over each region (mm day^{-1}) and associated PCs. Dashed lines are regional precipitation averages; solid lines are PCs. Correlation coefficients between PCs and averages are in the upper-right corner of each plot.

and the annual rainfall range is more than 5 mm day^{-1}. Based upon the concentration and intensity of the summer precipitation, regions 1, 2a, 3, 5, and 9 (Table 3) appear to make up the principal region of Asian monsoon influence. However, although these five regions have summer monsoon characteristics, low correlation coefficients between the monthly precipitation time series suggest they do not behave coherently.

Regions 2b, 7, and 8, representing south-central Asia (SCA), the Arabian Peninsula (AP), and central Asia (CA), respectively, are the driest regions and experience maximum precipitation in the winter and spring. Regions 4 and 6, the WEP and EEIO, respectively, are the wettest of the 10 regions. These near-equatorial regions have less precipitation seasonality compared to the other regions, although precipitation is highest in June and July in the western equatorial Pacific and in September through December in the eastern equatorial Indian Ocean. Correlation coefficients between the monthly regional precipitation time series are low, but there are significant correlations between summer precipitation (JJAS) in several regions (Table 4; Fig. 5). Some of the highest correlation coefficients are between the eastern equatorial Indian Ocean and ASM regions ($r = 0.64$), south-central Asia and

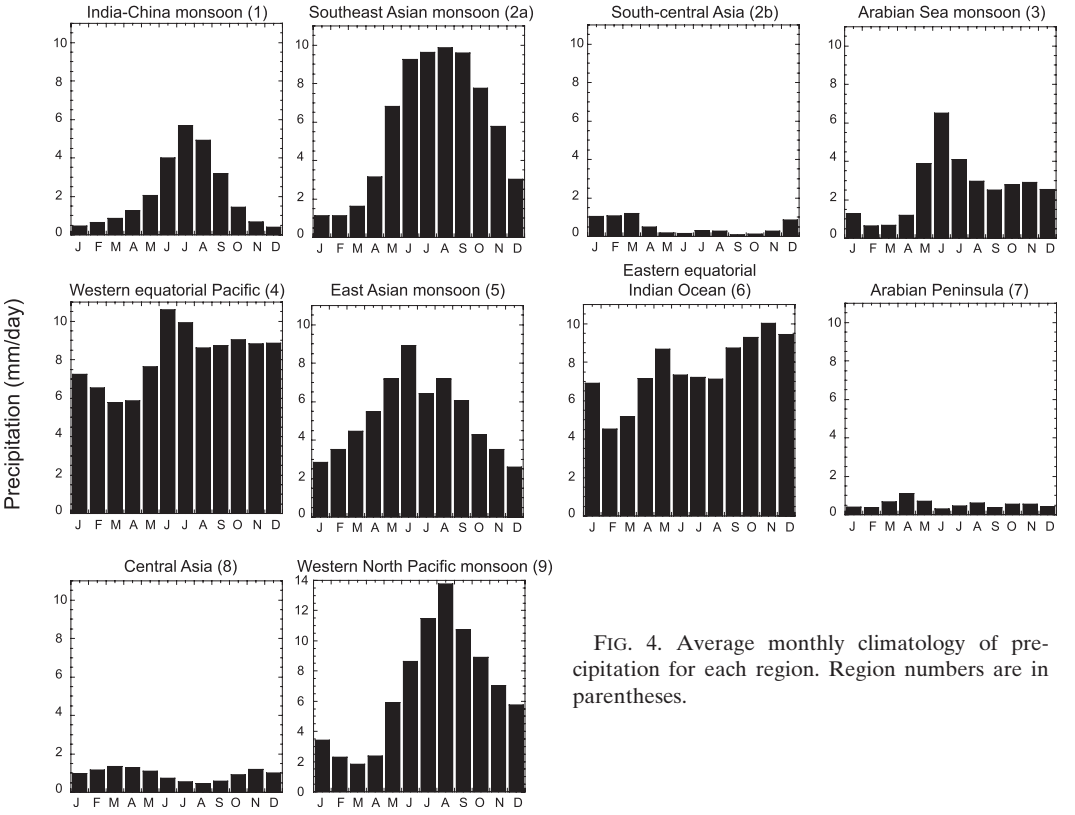

FIG. 4. Average monthly climatology of precipitation for each region. Region numbers are in parentheses.

the ASM region ($r = 0.59$), and the WNPM and ASM regions ($r = -0.47$). Thus, years with more summer precipitation over the Arabian Sea correspond to greater summer precipitation in the adjacent eastern equatorial Indian Ocean, as well as in south-central Asia. Yet when there is more summer precipitation in the Arabian Sea, there is less summer precipitation in the western North Pacific. Other regions with significant (but weaker) correlation coefficients are usually adjacent to one another: the Arabian Peninsula and south-central Asia ($r = 0.43$), and the eastern equatorial Indian Ocean and the SEAM region ($r = 0.44$).

To assess the spatial variability associated with strong and weak summer precipitation in each region, we created a set of maps that plots correlation coefficients between the regional summer precipitation time series and the time series of summer precipitation at each grid point (Fig. 5). Generally, we find significant positive correlations across each region. Aside from this result, one interesting pattern we observe is three prominent zones of correlation across the ICM region instead of one continuous region of positive correlation coefficients. These zones include one area over northern India, an area from the northern Bay of Bengal extending north into Tibet, and a band across the Korean Peninsula and Yellow Sea. Correlation maps also show a dipole pattern between the Arabian Sea and the western North Pacific that was already indicated by the negative correlation between the summer precipitation time series for these regions.

b. *Subregions of the Asian monsoon*

The ICM, ASM, SEAM, WNPM, and EAM regions comprise a region similar to Wang and LinHo's (2002) Asian monsoon region (Fig. 6), which they defined as the area with an annual rainfall range greater than 5 mm day^{-1} and more than 55% of the annual rainfall arriving between May and September. Since our regions

TABLE 3. Names given to the 10 CMAP regions defined by EOF analysis.

CMAP region	Name	Acronym
1	India-China monsoon	ICM
2a	Southeast Asian monsoon	SEAM
2b	South-central Asia	SCA
3	Arabian Sea monsoon	ASM
4	Western equatorial Pacific	WEP
5	East Asian monsoon	EAM
6	Eastern equatorial Indian Ocean	EEIO
7	Arabian Peninsula	AP
8	Central Asia	CA
9	Western North Pacific monsoon	WNPM

TABLE 4. Correlation coefficients of JJAS precipitation for each region and regions of Tibet (Fig. 11, described below). Values significant at the 95% confidence level are italicized. Values significant at the 99% confidence level are in boldface.

	ICM (1)	SEAM (2a)	SCA (2b)	ASM (3)	WEP (4)	EAM (5)	EEIO (6)	AP (7)	CA (8)	WNPM (9)
SEAM (2a)	*0.35*									
SCA (2b)	0.08	0.09								
ASM (3)	0.30	0.23	**0.59**							
WEP (4)	0.33	**0.44**	0.27	0.18						
EAM (5)	0.09	−0.21	−0.14	−0.14	−0.14					
EEIO (6)	0.19	0.17	0.26	**0.64**	*0.35*	−0.16				
AP (7)	0.05	0.25	**0.43**	*0.35*	0.09	0.00	0.20			
CA (8)	−0.18	0.16	0.05	0.27	−0.17	−0.06	0.01	0.23		
WNPM (9)	−0.15	−0.08	−0.07	**−0.47**	0.24	0.00	*−0.36*	0.10	−0.25	
Southeast Tibet	**0.71**	0.14	0.00	0.31	0.29	0.02	0.29	0.08	0.09	0.09
Southwest Tibet	**0.54**	**0.50**	0.08	0.20	0.11	0.10	0.08	0.31	−0.01	−0.17
Northwest Tibet	0.21	−0.14	−0.08	0.24	−0.23	0.20	0.15	0.17	**0.41**	0.03

are not based on the magnitude of seasonal precipitation, one key difference is that our Asian monsoon region also contains the Tibetan Plateau and more of northern China. Although these are arid continental regions, they are defined by monsoonal precipitation today and likely even more so in the past, when higher Northern Hemisphere summer insolation strengthened the Asian monsoon (Winkler and Wang 1993; Liu et al. 1998; Liu and Ding 1998). Wang and LinHo (2002) also defined three subsystems of the Asian monsoon: the Indian summer monsoon (ISM), western North Pacific summer monsoon (WNPSM), and the East Asian summer monsoon (EASM), based on both seasonal wind reversals and onset, peak, and withdrawal dates (Fig. 6). Similarly, the regions within our Asian monsoon domain have different onset, peak, and withdrawal characteristics. Summer precipitation begins in June, peaks in July, and lasts through September in the ICM region. In the SEAM region, summer precipitation begins more abruptly in May, with similar precipitation rates in June, July, August, and September. Withdrawal occurs in October. Summer precipitation also begins abruptly in May in the ASM region, peaks in June, and lasts only through July. The EAM region has a gradual onset of summer precipitation, with a peak in June, a decline in July, and a slight increase again in August. Precipitation begins in May, peaks in August, and declines gradually through the autumn months in the WNPM region. The WNPM region receives more precipitation in August than any other month relative to the other precipitation regions.

We compare our Asian monsoon subregions to the subsystems of Wang and LinHo (2002) in Fig. 6. Unlike the previous division of monsoon subsystems, our EOF-based regionalization does not reveal one coherent ISM region. Instead, the ASM region, which comprises southern India and the Arabian Sea, is separated from northern India (part of the ICM region), and the Bay of Bengal (part of the SEAM region). Spectral analyses of regional precipitation time series show a peak at 30 months in the ICM and SEAM regions (Fig. S4), suggestive of the quasi-biennial variability in the ISM region. A similar 30-month variance is also observed in the IMI (refer to Table 5 for list of acronyms for monsoon indices) of B. Wang et al. (2001). However, there is no significant power at 30 months in the ASM region. Our WNPM region clearly comprises the WNPSM region. Peak summer rainfall occurs in August, the same time as peak rainfall in the WNPSM region (Wang and LinHo 2002). Precipitation in our WNPM region has significant power in the 40–70-month band, similar to the 50-month periodicity that is also observed in the WNPSM index (B. Wang et al. 2001; Wang and LinHo 2002). Our EAM region spatially resembles the EASM region, although it does not reach as far north to include the Korean Peninsula and the East China Sea, likely because of the southward shift of the EASM rainbelt during the last few decades (Zhou et al. 2009). The rainfall peak in June, decline in July, and increase in August in the EAM region defines the monthly precipitation climatology of the EASM region (Wang and LinHo 2002; Ho et al. 2003). The decline in July is likely due to a stationary period in between northward jumps in the EASM frontal zone (Kripalani et al. 2007). Last, the SEAM region contains much of the ''transition zone'' or ''corridor'' region between the ISM and WNPSM (Fig. 5).

Correlations between our regional time series of summer precipitation with several published Asian monsoon indices also reveal which regions are responding to different monsoon subsystems (Tables 5, 6). Given that our ICM, ASM, and SEAM regions fall into the broad ISM region, it is not surprising that these three regions have the highest correlations with the AIRI and the IMI (Parthasarathy et al. 1994; B. Wang et al. 2001). Although south-central Asia does not have a strong summer monsoon signature, what little summertime moisture it receives

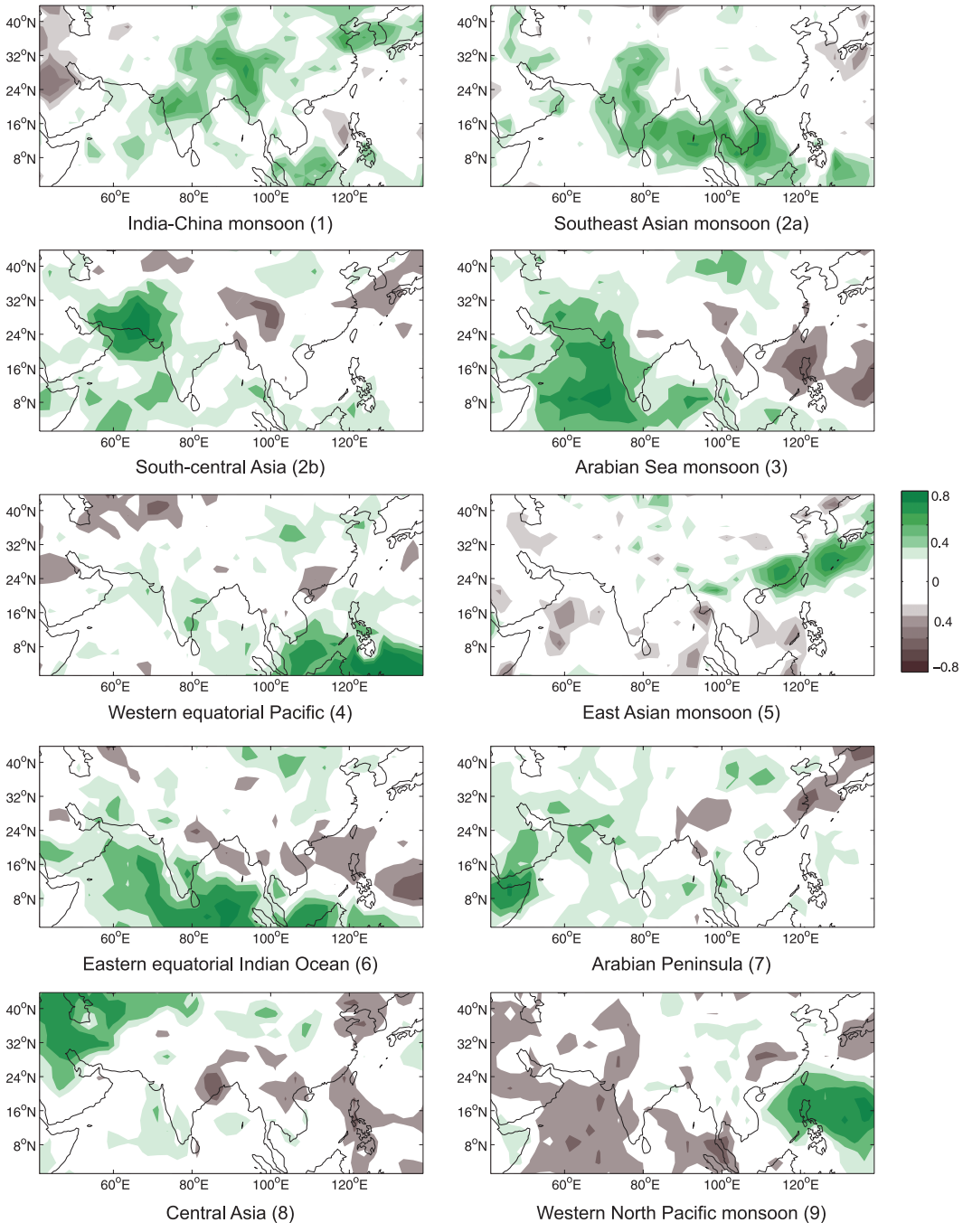

FIG. 5. Correlation map of annual, summed summer precipitation for each region and at each grid point. Correlation coefficients $> |0.35|$ are significant at the 95% confidence level.

is also correlated with these ISM indices. The ICM, ASM, and SEAM regions are also positively correlated with the MHI (Goswami et al. 1999), which is centered over Southeast Asia and India. The ASM and WNPM regions are also significantly correlated with the WYI and WNPMI (Webster and Yang 1992; B. Wang et al. 2001, 2008). Summer precipitation in the ASM region is inversely correlated with these indices, whereas the WNPM region has a positive correlation with the indices. Thus, again we observe that strong monsoon seasons in the WNP region are coincident with weaker monsoon seasons in the Arabian Sea. Our EAM region geographically resembles the EASM region, but it is not significantly correlated with either EASM index. This

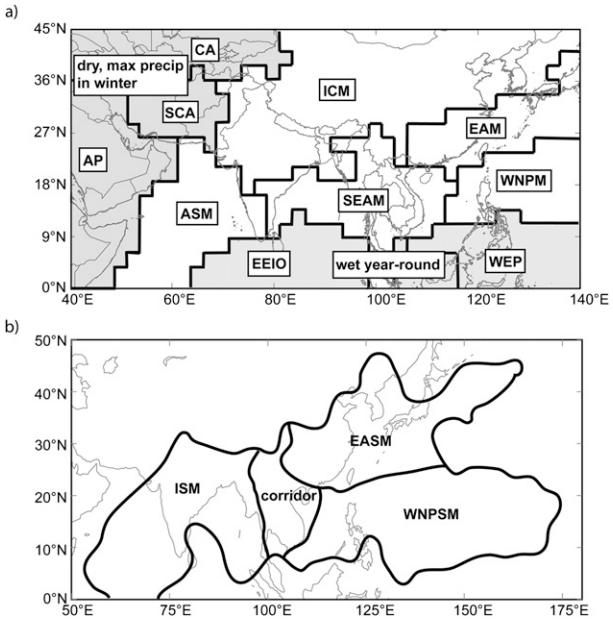

FIG. 6. (a) Asian monsoon region and subdomains defined from our analysis compared with (b) Asian monsoon region and subsystems of Wang and LinHo (2002).

may be because our EASM region is smaller than that of B. Wang et al. (2001), and it does not include as much of northeastern China and the Korean Peninsula. Or, the EASM indices we selected may not be appropriate, since they are not located directly over the area. The eastern equatorial Indian Ocean is wet year-round, with little precipitation seasonality, but JJAS precipitation here is also negatively correlated with the WNPMI. Thus, strong monsoon seasons in the WNP are also coincident with drier summer conditions in the equatorial Indian Ocean. The western equatorial Pacific, central Asia, and Arabian Peninsula regions are not significantly correlated with most of the Asian monsoon indices. This is not a surprising result because none of these regions presently has a monsoonal precipitation regime.

c. *Regional precipitation and local SST variability*

Local SST variability in the Indian Ocean and western Pacific Ocean can influence the hydrological cycle across the Asian monsoon region, causing changes in evaporation, precipitation, and circulation (Yang and Lau 2006). In the Indian Ocean, warm fall and winter SST is linked to stronger ISM precipitation and contributes to the biennial nature of the ISM (Meehl 1997; Clark et al. 2000). The Indian Ocean dipole (IOD) mode also drives changes in SST and precipitation across the Indian Ocean Basin (Saji et al. 1999; Ashok et al. 2004). Although a strong empirical relationship has been demonstrated between local SST and ISM variability, the mechanisms linking the two remain unclear, particularly in the Indian Ocean (Webster 2006). In the western Pacific, local SST variability also exerts an influence on precipitation in the EASM and WNPSM domains. Cooler SST in the WNP, together with anomalous anticyclonic circulation, typically leads to enhanced EASM precipitation and decreased WNPSM precipitation (Wang et al. 2000; Lau and Nath 2003).

To explore the relationship between SST and summer precipitation in each of our defined monsoon regions from Fig. 6 (we also include south-central Asia because it is significantly correlated with ISM indices), we created a set of maps depicting the correlation coefficients between regional summer precipitation and SST (Fig. 7). There are strong correlations between local SST and summer precipitation in several regions. More summer precipitation in the large ICM region occurs with higher SST in the Bay of Bengal, South China Sea (SCS), and Philippine Sea. Although warmer SST leads to increased evaporation and atmospheric moisture, this is a surprising result because previous studies indicate no concurrent

TABLE 5. List of Asian monsoon indices used in this analysis.

Index name	Variable	Reference
All-Indian rainfall index (AIRI)	JJAS summed rainfall over the Indian subcontinent	Parthasarathy et al. (1994)
Webster–Yang index (WYI)	Mean JJAS zonal wind shear between 850–200 mb for 0°–20°N, 40°–110°E.	Webster and Yang (1992)
Indian monsoon index (IMI)	Mean JJAS zonal wind difference at 850 mb between 5°–15°N, 40°–80°E and 20°30°N, 70°–90°E	B. Wang et al. (2001)
Monsoon Hadley index (MHI)	Mean JJAS meridional wind shear between 850 and 200 mb for 10°–30°N, 70°–110°E	Goswami et al. (1999)
Western North Pacific monsoon index (WNPMI)	Mean JJAS zonal wind difference at 850 mb between 5°–15°N, 100°–130°E and 20°–30°N, 110°–140°E	B. Wang et al. (2001)
EASM-SLP	Mean JJAS SLP for 10°–50°N, 110°–160°E	Zhou et al. (2009)
EASM-v850	Mean JJAS 850-mb meridional wind for 20°–45°N, 110°–120°E	Zhou et al. (2009); B. Wang et al. (2001)

TABLE 6. Correlation coefficients of JJAS precipitation for each region, regions of Tibet, and Asian monsoon indices. Values significant at 95% confidence level are in boldface.

	AIRI	IMI	MHI	WYI	WNPMI	EASM_SLP	EASM_v850
ICM (1)	**0.50**	**0.46**	**0.50**	0.13	−0.33	−0.23	**0.44**
SEAM (2a)	**0.40**	**0.42**	**0.39**	0.27	−0.24	0.11	0.34
SCA (2b)	**0.58**	**0.39**	0.30	−0.06	−0.16	−0.09	**0.36**
ASM (3)	**0.44**	**0.42**	**0.36**	**−0.42**	**−0.65**	−0.01	**0.38**
WEP (4)	0.32	0.28	0.09	0.35	−0.26	−0.01	0.30
EAM (5)	0.14	0.01	0.05	−0.03	−0.03	−0.32	0.25
EEIO (6)	0.19	0.17	0.11	−0.32	**−0.71**	−0.03	0.33
AP (7)	0.19	0.26	0.20	0.07	−0.01	−0.12	**0.45**
CA (8)	−0.05	−0.04	0.04	−0.10	−0.32	−0.12	0.04
WNPM (9)	−0.19	−0.20	−0.21	**0.45**	**0.56**	−0.19	−0.10
Southeast Tibet	0.17	0.12	0.23	0.05	**−0.37**	−0.26	0.32
Southwest Tibet	**0.40**	**0.58**	0.31	0.14	−0.06	0.03	0.33
Northwest Tibet	0.07	−0.11	−0.04	−0.22	−0.31	−0.30	0.16

relationship between Indian Ocean SST and ISM rainfall (Clark et al. 2000; Bollasina and Nigam 2009). Summer ASM precipitation is also positively correlated with SST in the Arabian Sea, Bay of Bengal, and SCS. In the EAM region, summer precipitation is negatively correlated with SST in the Arabian Sea, Bay of Bengal, and southern Indian Ocean, suggesting that cooler SST in these areas is coincident with enhanced EAM precipitation. In the WNPM region, summer precipitation is positively correlated with SST in the Arabian Sea and negatively correlated with SST off the coast of northern China and Japan. However, there is no correlation between WNP SST and WNP precipitation.

Previous studies have demonstrated a strong relationship between winter SST in the Indian Ocean and the strength of the subsequent ISM (Clark et al. 2000).

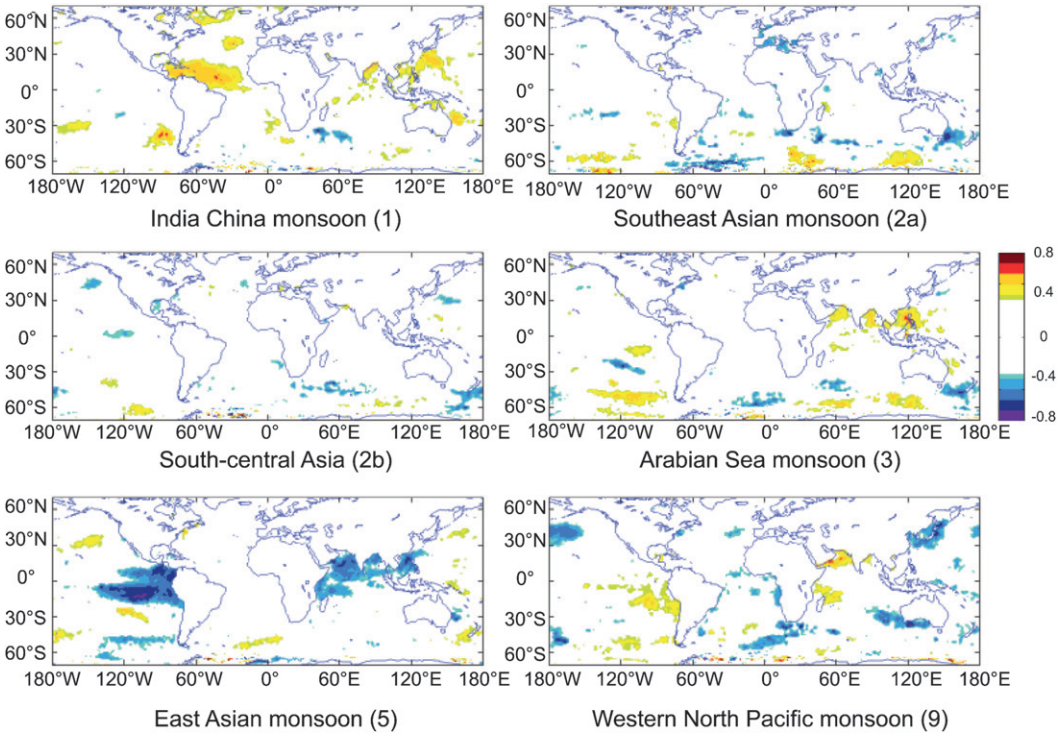

FIG. 7. Map of correlation coefficients for average JJAS HadISST (°C) and summed JJAS precipitation (mm season^{-1}) in each monsoon region, 1979–2009. Colored regions ($r > |0.35|$) are significant at the 95% confidence level.

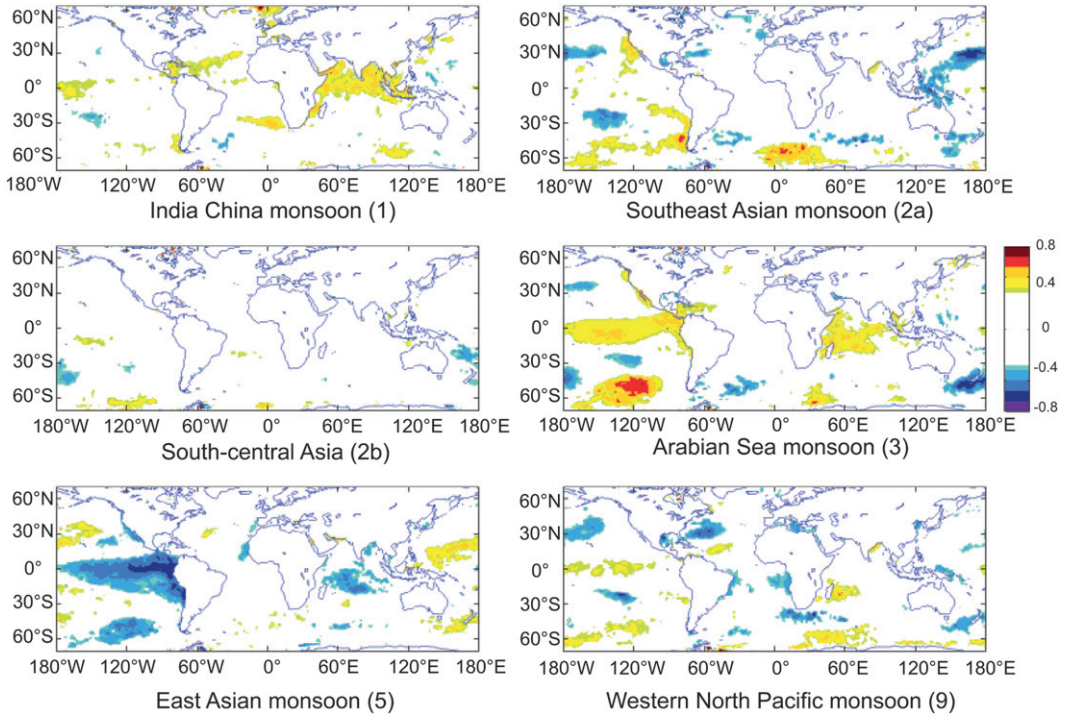

FIG. 8. Map of correlation coefficients for average DJFM HadISST (°C) and summed JJAS precipitation in each monsoon region, 1979–2009. Colored regions ($r > |0.35|$) are significant at the 95% confidence level.

We also find that correlation coefficients between winter [December–March (DJFM)] SST and summer precipitation are positive for the ICM region, indicating warmer SST the winter prior to enhanced summer precipitation, and vice versa (Fig. 8). Wintertime WNP SST also appears to be related to summertime precipitation variability in East and Southeast Asia. Wetter summers in the EAM region occur after winters with warmer SST in the WNP. SST in the southern Indian Ocean (SIO) also appears to influence summer precipitation variability. SIO SST is warmer the winter prior to wetter summers in the ASM region and cooler prior to wetter summers in the EAM region. The relationship between SIO wintertime SST and precipitation in the ASM region holds paleoclimatic significance, as Clemens and Prell (2003) have hypothesized that during the early Holocene, warm SIO SST was required, along with warmer Northern Hemisphere summer temperatures, to increase latent heat flux to the Northern Hemisphere and enhance ISM circulation. Based on our analysis, increased monsoon rainfall in the Arabian Sea is linked to warmer SIO SST.

d. Regional precipitation and remote SST variability

ENSO prominently influences SST in the Indian and western tropical Pacific Oceans, and drives interannual variability in ISM and EASM precipitation (Webster and Yang 1992; Webster et al. 1998; Lau and Nath 2003, 2006). However, interannual ENSO forcing is not coherent across all subsystems of the Asian monsoon (Wang et al. 2000). The ISM is weak as an El Niño event develops, but the WNPSM is weak after an El Niño event matures, whereas mei-yu precipitation is enhanced following El Niño events (Wang et al. 2000, 2001). Furthermore, the relationship between the ISM and ENSO varies on interdecadal time scales and has weakened during the last few decades (Kumar et al. 1999). Since the CMAP dataset begins in 1979, we are limited to analyzing a period with a weak ISM–ENSO relationship, and we do not observe strong correlation coefficients between precipitation in ISM-influenced regions and tropical Pacific SST (Figs. 7, 8). However, Figs. 7 and 8 suggest that increased summer precipitation in the EAM region coincides with cool SST anomalies in the eastern and central tropical Pacific the winter before the summer monsoon, as well as during the monsoon season. Of the seven (upper quartile) summers with the most summer precipitation in the EAM region (2008, 1997, 2000, 1998, 2002, 2001, 1999), only two are El Niño years, and 1998–2002 encompasses a large La Niña event. Summer precipitation in the ASM region is positively correlated with winter SST in the central and eastern tropical Pacific (Fig. 8). ENSO is a likely link between the SIO, Arabian Sea precipitation, and the dipole relationship between ASM precipitation

and WNPM precipitation. El Niño events drive warmer wintertime SST into the southwest Indian Ocean, which we observe leads to wetter summers in the Arabian Sea (Annamalai et al. 2005). Warmer Indian Ocean SST also induces an anomalous anticyclonic circulation anomaly in the Philippine Sea, leading to reduced WNP precipitation (Lau and Nath 2000; Annamalai et al. 2005; Du et al. 2011).

Instrumental observations and climate model simulations suggest that climate in the North Atlantic also influences Asian monsoon precipitation on interdecadal time scales, with colder North Atlantic SST causing weaker precipitation in the ISM and EASM regions (Goswami et al. 2006; Zhang and Delworth 2006; Feng and Hu 2008). This relationship has also been observed on longer time scales (e.g., Gupta et al. 2003; Wang et al. 2005). The atmospheric link between these two regions may lie in changes in the meridional tropospheric temperature gradient in the Asian monsoon region. With warmer North Atlantic SST, tropospheric temperature increases in the Northern Hemisphere. This enhances the meridional temperature gradient between the Southern and Northern Hemispheres, leading to enhanced monsoonal circulation, ISM rainfall, and a longer ISM season (Goswami et al. 2006). Alternately, Feng and Hu (2008) propose that it is the warming of the troposphere over the Tibetan Plateau during periods of warmer North Atlantic SST that enhances the ISM, something that may have occurred on longer time scales as well (Overpeck et al. 1996). Or, warmer North Atlantic SST may cause a northward shift of the ITCZ, increasing convergence over the ISM region (Zhang and Delworth 2006). We find that interannual-scale summer precipitation variability in the ICM region is highly correlated with JJAS SST in the North Atlantic Ocean, supporting the link between North Atlantic climate and Asian monsoon variability. There is no relationship between North Atlantic SST and summer precipitation for the four other monsoon subregions. However, the short length (31 yr) of our time series limits a discussion of the relationship between lower-frequency changes in monsoon precipitation and North Atlantic variability.

e. Regional precipitation and atmospheric variability

SLP and 850-mb winds are useful representations of monsoon circulation strength near the surface (Lau and Nath 2000). During the monsoon season, SLP is typically low across much of the monsoon region, indicating enhanced moisture convergence. Strong southwesterly monsoon winds characterize the Arabian Sea, transporting moisture into India, while southwesterly flow in the Bay of Bengal and South China Sea, coupled with southeasterly flow in the WNP, transports moisture north into China. To assess the atmospheric variability associated with anomalously wet and dry summers in each monsoon region, we created a set of composite maps of average SLP and 850-mb wind anomalies for the seven wettest (top quartile) and seven driest (bottom quartile) summers, discussed in the subsequent paragraphs (Figs. 9, 10).

During wet summers in the ICM region, SLP is lower over the Arabian Peninsula compared to the long-term summer mean. There is also a high SLP anomaly over the Tibetan Plateau and the Philippine Sea, accompanied by anticyclonic flow. This Philippine Sea SLP anomaly pattern is reversed during dry years. Wang et al. (2000) and Lau and Nath (2003) observed a similar feature when looking at the atmospheric impact of ENSO in the Asian monsoon region, dubbed the Philippine Sea anticyclone (PSAC). Warm SST anomalies during El Niño events produce Gill-type atmospheric Rossby waves, which, through local air–sea interactions, lead to the development of an anomalous anticyclone and high SLP over the Philippine Sea. The PSAC typically develops in the fall and winter months and persists into the summer months. Despite the observed PSAC anomaly, we did not observe a relationship between ICM precipitation and tropical Pacific SST. SST variability in the southwestern Indian Ocean may also contribute to the development of the PSAC, linking Arabian Sea precipitation, which is highly correlated with southwestern Indian Ocean SST, and WNP precipitation (Annamalai et al. 2005). Southwesterly monsoon winds on the western edge of the Arabian Sea are stronger during wet ICM summers, and the PSAC leads to more onshore winds into the southern part of the ICM region, indicating that increased summer precipitation in this region is due to an increase in moisture flux from both the Pacific and Indian Oceans.

The SEAM region experiences anomalous onshore easterly winds in wet summers, resulting from a PSAC-type anomaly northeast of the region. Because winds are typically southwesterly here in the summer months, this composite map suggests that summers with increased precipitation may be due to increased moisture flux from the WNP, rather than the Bay of Bengal. Dry SEAM summers are accompanied by anomalously low SLP just north of the typical PSAC region, as well as anomalously high SLP in the Arabian Sea. In the ASM region and south-central Asia, low SLP anomalies occur over the Arabian Sea during wet summers. Southeasterly flow along the northern edge of this SLP anomaly likely transports more Bay of Bengal moisture to south-central Asia during wet summers. The southwesterly monsoon winds in the Arabian Sea are actually weaker during wet summers in the ASM region. The PSAC is also present during wet summers in the ASM region, leading to the

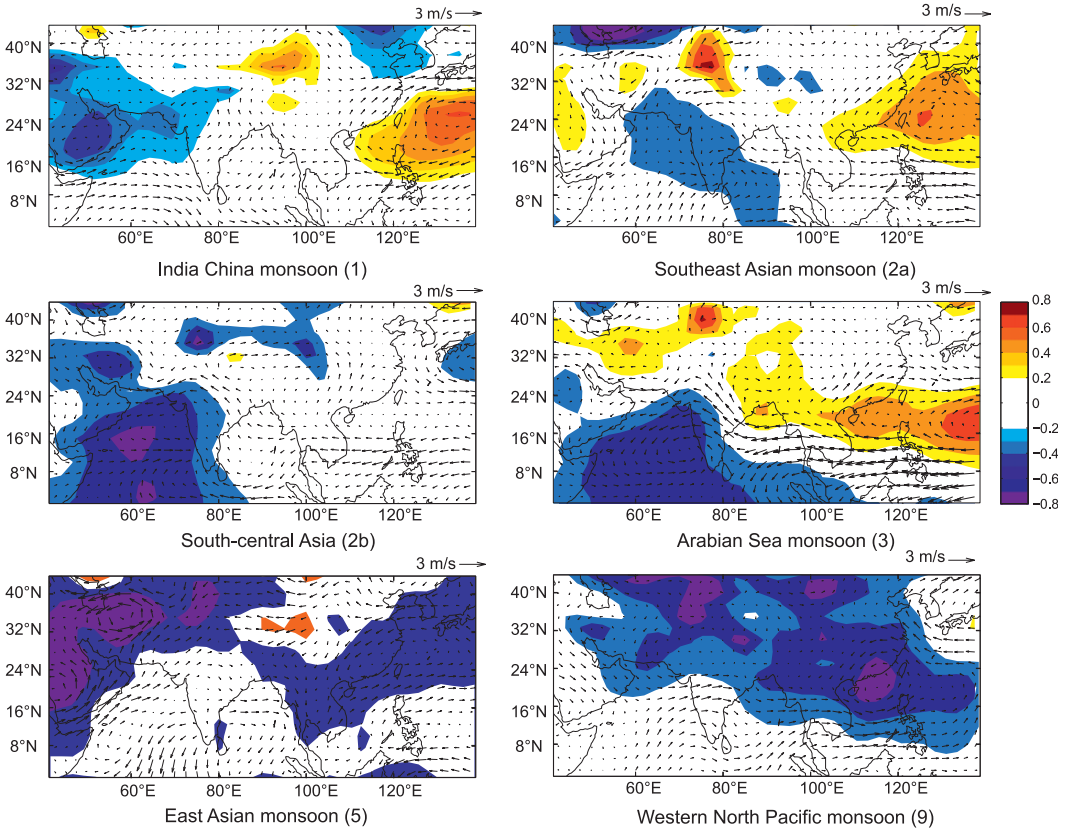

FIG. 9. Composite map of 850-mb vector wind anomalies (arrows) and SLP (contours) for the seven wettest summers in each monsoon region.

observed dipole between summer precipitation in the Arabian Sea and WNP. This pattern is reversed during dry ASM summers.

In the EAM region, anomalously low SLP and southeasterly flow transports more tropical moisture from the WNP northward, and eventually landward, during wet summers. SLP is also anomalously low over the Arabian Peninsula and south-central Asia in years with increased summer precipitation, and vice versa. During dry EAM summers, there is anomalous offshore flow at ~32°N, which likely reduces moisture flux into the region. The WNPM region experiences low SLP during wet summers. These low SLP anomalies also extend over much of the Asian continent from 60° to 120°E. However, there are no apparent SLP anomalies or strong changes in winds during dry WNPM summers. Yet, SLP is higher over the Arabian Sea, which again fits with our observation of decreased Arabian Sea precipitation coinciding with enhanced WNP precipitation.

f. Paleomonsoon records and EOF-defined regions

Numerous paleoclimate records infer past changes in monsoon variability within our Asian monsoon subregions. However, many of these records fall outside the previously published boundary of Asian monsoon influence, such as records from the arid Tibetan Plateau. Furthermore, not all monsoon paleorecords show coherent precipitation variability during the Holocene, which complicates our understanding of past monsoon dynamics. Our analysis suggests that some of the discrepancies between Asian monsoon paleorecords may be due to their location in regions that experience different precipitation regimes, and other studies have also noted regional differences in Asian monsoon paleorecords. Comparing monsoon paleorecords from across the traditional ISM region, Staubwasser (2006) defined three regions with distinctive precipitation variability during the Holocene: (i) the Ganges-Brahmaputra catchment, extending south to the Bay of Bengal, experienced peak rainfall during the early-to mid-Holocene and subsequent weakening through the late Holocene; (ii) the northwestern Indus catchment does not show such a trend; and (iii) the Western Ghats, in southwestern India, show an increasing precipitation trend in the late Holocene. Interestingly, these three regions also reflect our EOF-based precipitation boundaries: the Ganges-Brahmaputra catchment is part

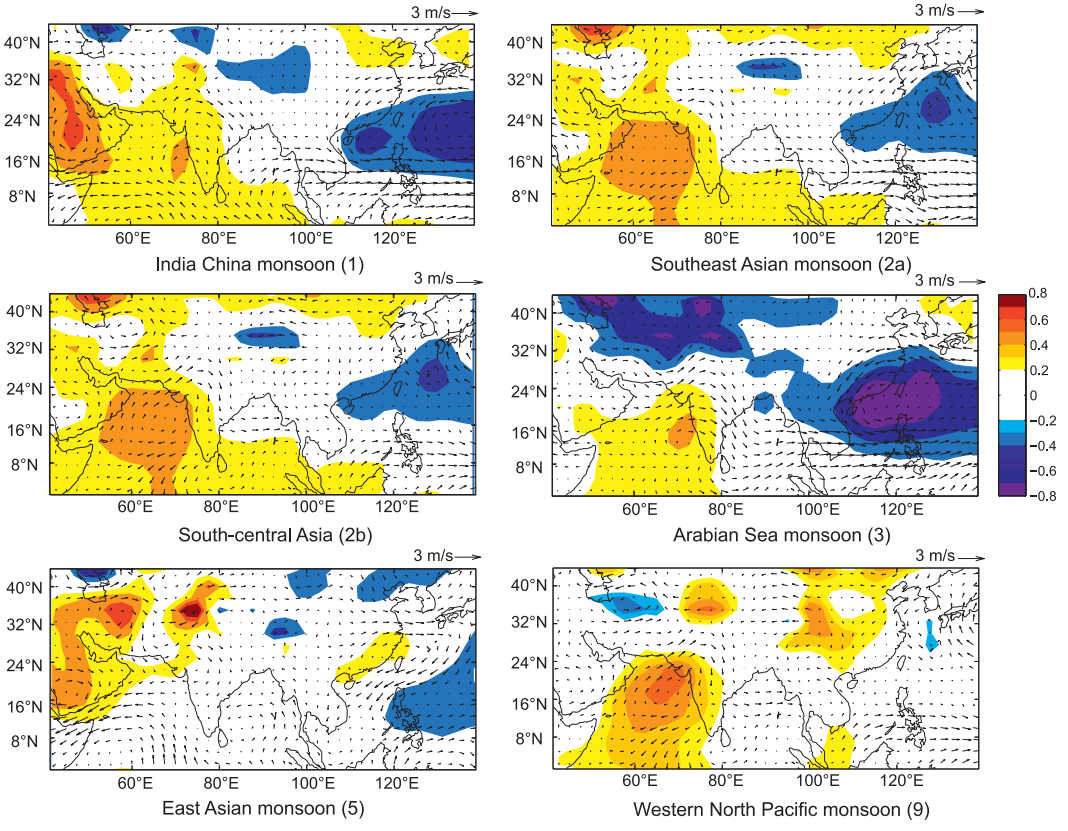

FIG. 10. As in Fig. 9, but for the seven driest summers in each monsoon region.

of the ICM region, the Indus catchment falls into our south-central Asia region, and the Western Ghats are located in the ASM region. During the 31 yr of CMAP data, summer precipitation across these regions does not covary strongly. A similar lack of coherency on millennial time scales suggests that our regionalization scheme may be relevant at longer time scales.

Other studies have noted regional differences in the timing of maximum monsoon moisture across China (An et al. 2000; He et al. 2004). Peak Holocene monsoon strength inferred from numerous paleoclimate reconstructions divides China into three zones: (i) in northern and western China, precipitation peaked from 10 to 7 ka (ka = kiloannum = 1000 yr); (ii) in southeastern China, peak precipitation occurred between 6 and 3 ka; and (iii) in southwestern China, peak precipitation was earlier, ~11 ka (An et al. 2000). The timing of peak Holocene summer monsoon strength is hypothesized to have occurred progressively later in more southern locations, reflecting an equatorward shift in the EASM front due to the decline in maximum NH summer insolation (An et al. 2000). An earlier peak in southwestern China is attributed to this region responding more to the ISM than the EASM (An et al. 2000). However, the temporal boundaries of maximum monsoon moisture inferred from paleorecords also coincide with our regional boundaries. Across the Tibetan Plateau and northern China (within the ICM region), peak monsoon moisture occurred between 10 and 5 ka, similar to the timing of peak monsoon moisture in the Ganges-Brahmaputra catchment, also part of the ICM region (Wei and Gasse 1999; An et al. 2000; Staubwasser 2006; Mügler et al. 2010). Monsoon paleorecords from within our defined EAM domain indicate peak monsoon moisture occurred between 3 and 6 ka, whereas paleorecords from southwestern China (part of the SEAM region) show peak monsoon moisture at 11 ka (An et al. 2000). Thus, despite some geochronological uncertainty, these different regional timings of maximum monsoon moisture may be another climatic characteristic reflecting the presence of unique precipitation regimes across the Asian monsoon region.

Many of the longest, best-dated paleorecords of past monsoon variability come from speleothem-derived oxygen isotopes (Y. J. Wang et al. 2001, 2005; Dykoski et al. 2005; Cosford et al. 2008; Fleitmann et al. 2007; Y. J. Wang et al. 2008). Although some of these caves are thousands of kilometers apart, millennial-scale changes

within their inferred monsoon paleorecords often show similar variability, including abrupt shifts coherent with North Atlantic climate events, peak Asian monsoon strength in the early Holocene, and a gradual decline in inferred monsoon strength in the mid-Holocene. Many of these speleothem records are found in the ICM region. Although we would expect precipitation paleorecords from across this region to be coherent, the similarity among records from central China, the EASM region of China, and Oman is challenging to interpret because our modern precipitation analysis suggests that summer precipitation does not covary in these regions.

Recent observational analyses of stable water isotope values, precipitation, and temperature suggest that speleothem isotope records may reflect the influence of factors other than changes in summer precipitation amount, such as changing seasonality and moisture trajectories (Dayem et al. 2010). A new simulation from an isotope-embedded GCM suggests that the observed temporal similarity between speleothem records across the Asian monsoon region may be due to changes in water vapor transport rather than precipitation amount (LeGrande and Schmidt 2009). This hypothesis may explain why speleothems infer a gradual decline in precipitation during the Holocene, but other monsoon records, such as those derived from lake sediments, (which likely recorded precipitation amount) indicate more abrupt shifts and less coherence on millennial time scales (Overpeck and Cole 2006). However, the extrapolation of our defined regions to longer time scales is fraught with uncertainty because of the short length of the precipitation dataset used in this study. Future EOF-based regionalization analyses on paleoprecipitation records and model simulations will provide more insight into the stability of these regional precipitation regimes on longer time scales.

g. Tibetan Plateau precipitation regionalization

Many paleoclimate records of inferred Asian monsoon variability come from Tibetan lake sediments, ice cores, and tree rings (Gasse et al. 1991, 1996; Thompson et al. 1997; Liu et al. 1998; Thompson et al. 2000; Bräuning and Mantwill 2004; Morrill et al. 2006; Shen et al. 2008a,b; Mischke et al. 2008; X. C. Wang et al. 2008; Tang et al. 2009). Although the Tibetan Plateau receives most of its precipitation in the summer months, it is now extremely arid relative to other monsoonal regions and is not included within the boundary of Asian monsoon influence defined by the instrumental record (Wang and LinHo 2002). Yet, paleoclimate references often draw the boundary of Asian monsoon influence somewhere over the Tibetan Plateau (Winkler and Wang 1993; Herzschuh 2006; Morrill et al. 2006), but this boundary is often qualitative. The most quantitative work to date on the maximum extent of monsoon influence in Tibet is based on stable isotopes of precipitation from a handful of short station records. These records indicate the monsoonal moisture boundary lies at ~35°N (Tian et al. 2001). In our analysis, Tibet is part of the ICM region, an area that extends much farther north and west than previously defined monsoon boundaries. This would imply that the numerous inferred precipitation paleorecords from the plateau, including those north of 35°N, should reflect summer monsoon variability. Furthermore, based on our regionalization, interpretations of past increases in summer moisture in Tibet should be interpreted as increases in the amount of monsoonal precipitation, rather than a northward shift in the monsoon boundary. Interestingly, and in contrast, the monsoon domain may have shifted onto the Arabian Peninsula earlier in the Holocene and exited in the second half of the Holocene until present (Overpeck et al. 1996; Fleitmann et al. 2007).

However, the ICM region comprises the largest area in our regionalization scheme, and there is almost certainly strong regional precipitation variability within its boundaries. Given this fact, and our desire to define the northwestern limit of monsoon moisture more quantitatively over the Tibetan Plateau, we performed an EOF-based regionalization of the 98 CMAP precipitation grid points from 28°–44°N, 75°–105°E (Fig. 11). This area extends slightly beyond the boundaries of the Tibetan Plateau and is mostly contained in the ICM region. Based on the same significance tests used in the original regionalization, we decided to retain and rotate three eigenvectors, explaining 95.6% of the total variance.

The three resulting EOFs divide the plateau into three sectors: the southeast (EOF1-SE), northwest (EOF2-NW), and southwest (EOF3-SW). The southeast and southwest regions fall into the ICM region, and the northwest region straddles central Asia and the ICM region (Fig. 11). Summed, summer precipitation (JJAS) in the southeast and southwest is positively correlated with summer ICM precipitation, and summer precipitation in the northwest is positively correlated with summer precipitation in central Asia (Table 3). All the Tibetan regions have most of their precipitation in the summer months, with precipitation peaking in July, explaining their inclusion in the ICM region. However, the northwest region is much drier. The latitudinal boundary between the northwest and southeast–southwest regions lies at ~36°N, very close to the stable isotope monsoon boundary described by Tian et al. (2001). The summer peak in precipitation in the northwest region still suggests a monsoonal climate compared to

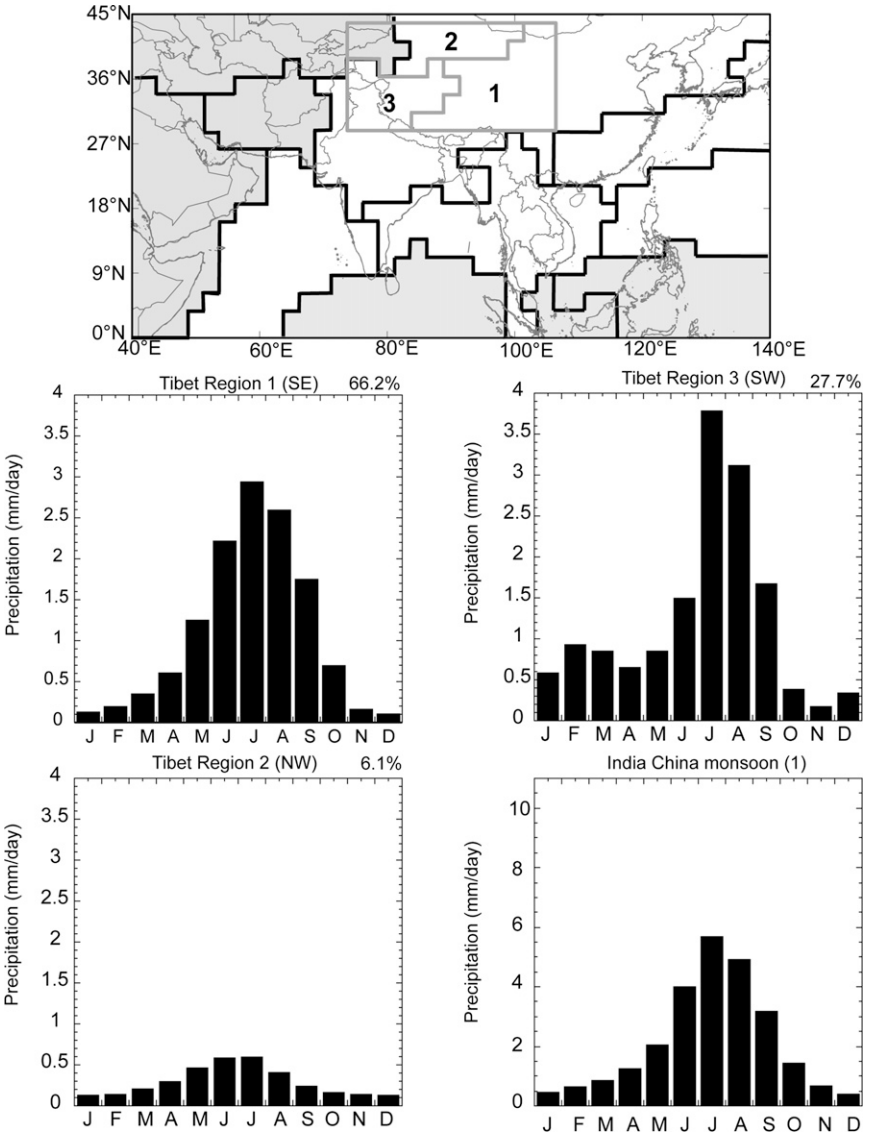

FIG. 11. Regionalization of Tibetan Plateau precipitation, with monthly climatology for each region as well as the ICM region. Percent variance explained by each eigenvalue is in right corner of each precipitation plot.

central Asia, which has peak precipitation in the winter and spring months. However, the northwestern Tibetan Plateau may have a different precipitation source (e.g., continental water recycling), although it has similar precipitation seasonality as regions farther south (Tian et al. 2001).

Correlations between summer precipitation in each Tibet region and the monsoon indices indicate that only the southwest region of Tibet has a relationship with the ISM, whereas the southeast region has a significant negative correlation with the WNPSM (Table 5). The negative correlation between the southeast Tibetan Plateau precipitation and the WNPSMI implies that a stronger WNPSM is coincident with reduced summer precipitation farther north, similar to the conclusions of B. Wang et al. (2008), who note that a strong WNPSM coincides with a weaker EASM. Thus, precipitation paleorecords from the southwest region of the plateau may not be responding to the same monsoon subsystem as precipitation paleorecords from the southeast region of the plateau.

6. Conclusions

Precipitation across the Asian monsoon region is far from homogenous. We have identified 10 regions of

unique precipitation variability within this area. Five of these regions comprise the Asian monsoon domain that extends from the Arabian Sea to the western North Pacific, similar to the boundary defined by Wang and LinHo (2002). However, because our analysis is not based on the magnitude of precipitation, there are some key differences, notably the inclusion of the Tibetan Plateau, northern China, and even southern Mongolia in the Asian monsoon domain.

Our Asian monsoon subdomains are also similar to those defined by Wang and LinHo (2002) and represent the WNPSM, the EASM, and a Southeast Asian ''corridor'' region between the major monsoon subsystems. However, the traditional ISM region is segmented because the Arabian Sea has distinctive precipitation variability relative to much of India and China. Mean summer wind direction and plots of composite wind anomalies suggest that our ICM region is a hybrid region, influenced by moisture from both the Indian and Pacific Oceans. The limited summer precipitation in south-central Asia is correlated with the ISM, although the region does not have a monsoonal climate. Decomposing gridded precipitation on the Tibetan Plateau into three regions indicates that only the southwest region of the plateau responds to the ISM, whereas the southeast region has an inverse relationship with the WNPSM. Some of our regions do have coherent summer precipitation. More notable is the dipole between summer precipitation in the Arabian Sea and the WNP. The mechanism responsible for this dipole likely involves ENSO, which modulates precipitation in these two regions through the warming of southwest Indian Ocean SST and the development of the PSAC (Annamalai et al. 2005).

Precipitation variability in each region is closely related to atmospheric and oceanic variability. Local SST influences precipitation in all our monsoon regions, and more remote ENSO variability in the tropical Pacific appears to impact precipitation in several regions, particularly through the development of the PSAC. It is also clear that not every region responds similarly to ENSO forcing, Thus, on shorter (i.e., interannual) time scales, precipitation paleorecords in different monsoon subsystems may not covary because of different responses to internal forcing (Wang et al. 2003). Our analysis suggests that potential summer precipitation paleorecords from the western equatorial Pacific, eastern equatorial Indian Ocean, central Asia, and Arabian Peninsula should not be immediately interpreted as proxies for Asian monsoon strength without calibration with the instrumental record, as these regions are currently not defined by a monsoonal climatology. However, as seen by the maps of precipitation correlations, the boundaries of our regions are not rigid and some proxies located on or beyond these boundaries could respond to monsoon precipitation. One caveat of this analysis is that this regionalization is based on only three decades of data and may change with additional data and with different time scales, forcing factors, and background conditions. For example, when the Asian monsoon was stronger in the early Holocene, regions of coherent precipitation variability could have extended even farther west, or differed in other ways. Future investigations could employ a similar regionalization scheme on model simulations at different times in the past, or on spatial field reconstructions of past hydrologic variability, such at the *Monsoon Asia Drought Atlas* (Cook et al. 2010a,b).

With future increases in greenhouse gas concentrations, the amount, location, and timing of Asian monsoon precipitation may also change in regionally distinct ways, although it is still unclear whether monsoon precipitation across Asia will increase or decrease because of differing model projections and biases (Meehl and Arblaster 2003; Meehl et al. 2007; Annamalai et al. 2007; Kripalani et al. 2007; Ashfaq et al. 2009). Future precipitation changes across the Asian monsoon domain may also lead to different monsoon subdomains. Treydte et al. (2006) has already observed a coherent trend of increasing precipitation in the last 100 years across the ISM region, the EASM region, and Pakistan, suggesting that the greenhouse-gas-induced intensification of the hydrologic cycle may force some of our defined regions of distinct precipitation variability to behave more coherently in the future.

Acknowledgments. This research was funded in part by NSF SBD-HSD Grant 0611320. Special thanks are given to The University of Arizona's Department of Geosciences for additional funding. We also thank J. E. Cole, J. Russell, A. Cohen, M. E. Evans, N. McKay, D. Thompson, and T. Ault for their helpful discussion and useful comments.

REFERENCES

Abram, N. J., M. K. Gagan, Z. Y. Liu, W. S. Hantoro, M. T. McCulloch, and B. W. Suwargadi, 2007: Seasonal characteristics of the Indian Ocean dipole during the Holocene epoch. *Nature,* **445,** 299–302.

Adler, R. F., and Coauthors, 2003: The Version-2 Global Precipitation Climatology Project (GPCP) monthly precipitation analysis (1979–present). *J. Hydrometeor.,* **4,** 1147–1167.

Agnihotri, R., K. Dutta, R. Bhushan, and B. L. K. Somayajulu, 2002: Evidence for solar forcing on the Indian monsoon during the last millennium. *Earth Planet. Sci. Lett.,* **198,** 521–527.

Ahmad, S. M., G. A. Babu, V. M. Padmakumari, and W. Raza, 2008: Surface and deep water changes in the northeast Indian

Ocean during the last 60 ka inferred from carbon and oxygen isotopes of planktonic and benthic foraminifera. *Palaeogeogr. Palaeoclimatol. Palaeoecol.,* **262,** 182–188.

An, Z., S. C. Porter, J. E. Kutzbach, W. Xihao, W. Suming, L. Xiaodong, L. Xiaoqiang, and Z. Weijian, 2000: Asynchronous Holocene optimum of the East Asian monsoon. *Quat. Sci. Rev.,* **19,** 743–762.

Anderson, D. M., J. T. Overpeck, and A. K. Gupta, 2002: Increase in the Asian southwest monsoon during the past four centuries. *Science,* **297,** 596–599.

Annamalai, H., P. Liu, and S. P. Xie, 2005: Southwest Indian Ocean SST variability: Its local effect and remote influence on Asian monsoons. *J. Climate,* **18,** 4150–4167.

——, K. Hamilton, and K. R. Sperber, 2007: The South Asian summer monsoon and its relationship with ENSO in the IPCC AR4 simulations. *J. Climate,* **20,** 1071–1092.

Ashfaq, M., Y. Shi, W.-W. Tung, R. J. Trapp, X. Gao, J. S. Pal, and N. S. Diffenbaugh, 2009: Suppression of South Asian summer monsoon precipitation in the 21st century. *Geophys. Res. Lett.,* **36,** L01704, doi:10.1029/2008GL036500.

Ashok, K., Z. Y. Guan, N. H. Saji, and T. Yamagata, 2004: Individual and combined influences of ENSO and the Indian Ocean dipole on the Indian summer monsoon. *J. Climate,* **17,** 3141–3155.

Bollasina, M., and S. Nigam, 2009: Indian Ocean SST, evaporation, and precipitation during the South Asian summer monsoon in IPCC-AR4 coupled simulations. *Climate Dyn.,* **33,** 1017–1032.

Bräuning, A., and B. Mantwill, 2004: Summer temperature and summer monsoon history on the Tibetan Plateau during the last 400 years recorded by tree rings. *Geophys. Res. Lett.,* **31,** L24205, doi:10.1029/2004GL020793.

Buckley, B. M., K. Palakit, K. Duangsathaporn, P. Sanguantham, and P. Prasomsin, 2007: Decadal scale droughts over northwestern Thailand over the past 448 years: Links to the tropical Pacific and Indian Ocean sectors. *Climate Dyn.,* **29,** 63–71.

Buell, C. E., 1979: On the physical interpretation of empirical orthogonal functions. Preprints, *Sixth Conf. on Probability and Statistics in Atmospheric Sciences,* Banff, AB, Canada, Amer. Meteor. Soc., 112–117.

Cai, Y. J., Z. An, H. Cheng, R. L. Edwards, M. J. Kelly, W. Liu, X. Wang, and C.-C. Shen, 2006: High-resolution absolute-dated Indian monsoon record between 53 and 36 ka from Xiaobailong Cave, southwestern China. *Geology,* **34,** 621–624.

Caratini, C., I. Bentaleb, M. Fontugne, M. T. Morzadec-Kerfourn, J. P. Pascal, and C. Tissot, 1994: A less humid climate since ca. 3500 yr B.P. from marine cores off Karwar, western India. *Palaeogeogr. Palaeoclimatol. Palaeoecol.,* **109,** 371–384.

Cattell, R. B., 1966: The scree test for the number of factors. *Multivariate Behav. Res.,* **1,** 245–276.

Clark, C. O., J. E. Cole, and P. J. Webster, 2000: Indian Ocean SST and Indian summer rainfall: Predictive relationships and their decadal variability. *J. Climate,* **13,** 2503–2519.

Clemens, S. C., and W. L. Prell, 2003: A 350,000 year summer-monsoon multi-proxy stack from the Owen Ridge, northern Arabian Sea. *Mar. Geol.,* **201,** 35–51.

——, and ——, 2007: The timing of orbital-scale Indian monsoon changes. *Quat. Sci. Rev.,* **26,** 275–278.

Clift, P. D., and R. A. Plumb, 2008: *The Asian Monsoon: Causes, History and Effects*. Cambridge University Press, 270 pp.

Colman, S. M., S. Y. Yu, Z. An, J. Shen, and A. C. G. Henderson, 2007: Late Cenozoic climate changes in China's western interior: A review of research on Lake Qinghai and comparison with other records. *Quat. Sci. Rev.,* **26,** 2281–2300.

Comrie, A. C., and E. C. Glenn, 1998: Principal components-based regionalization of precipitation regimes across the southwest United States and northern Mexico, with an application to monsoon precipitation variability. *Climate Res.,* **10,** 201–215.

Cook, E. R., K. J. Anchukaitis, B. M. Buckley, R. D. D'Arrigo, G. C. Jacoby, and W. E. Wright, 2010a: Asian monsoon failure and megadrought during the last millennium. *Science,* **328,** 486–489.

——, ——, ——, ——, ——, and ——, 2010b: LDEO TRL monsoon Asia drought atlas. [Available online at http://iridl.ldeo.columbia.edu/SOURCES/.LDEO/.TRL/.MADA/.]

Cosford, J., H. R. Qing, B. Eglington, D. Mattey, D. X. Yuan, M. L. Zhang, and H. Cheng, 2008: East Asian monsoon variability since the mid-Holocene recorded in a high-resolution, absolute-dated aragonite speleothem from eastern China. *Earth Planet. Sci. Lett.,* **275,** 296–307.

Cullen, H. M., P. B. deMenocal, S. Hemming, G. Hemming, F. H. Brown, T. Guilderson, and F. Sirocko, 2000: Climate change and the collapse of the Akkadian empire: Evidence from the deep sea. *Geology,* **28,** 379–382.

Dayem, K. E., P. Molnar, D. S. Battisti, and G. H. Roe, 2010: Lessons learned from oxygen isotopes in modern precipitation applied to interpretation of speleothem records of paleoclimate from eastern Asia. *Earth Planet. Sci. Lett.,* **295,** 219–230.

Denniston, R. F., L. A. Gonzalez, Y. Asmerom, R. H. Sharma, and M. K. Reagan, 2000: Speleothem evidence for changes in Indian summer monsoon precipitation over the last ~2300 years. *Quat. Res.,* **53,** 196–202.

Ding, Y. H., and J. C. L. Chan, 2005: The East Asian summer monsoon: An overview. *Meteor. Atmos. Phys.,* **89,** 117–142.

Du, Y., L. Yang, and S.-P. Xie, 2011: Tropical Indian Ocean influence on northwest Pacific tropical cyclones in summer following strong El Niño. *J. Climate,* **24,** 315–322.

Dykoski, C. A., and Coauthors, 2005: A high-resolution, absolute-dated Holocene and deglacial Asian monsoon record from Dongge Cave, China. *Earth Planet. Sci. Lett.,* **233,** 71–86.

Feng, S., and Q. Hu, 2008: How the North Atlantic multidecadal oscillation may have influenced the Indian summer monsoon during the past two millennia. *Geophys. Res. Lett.,* **35,** L01707, doi:10.1029/2007GL032484.

Fleitmann, D., and Coauthors, 2007: Holocene ITCZ and Indian monsoon dynamics recorded in stalagmites from Oman and Yemen (Socotra). *Quat. Sci. Rev.,* **26,** 170–188.

Gadgil, S., 2003: The Indian monsoon and its variability. *Annu. Rev. Earth Planet. Sci.,* **31,** 429–467.

Gasse, F., and Coauthors, 1991: A 13,000-year climate record from western Tibet. *Nature,* **353,** 742–745.

——, J. Ch. Fontes, E. Van Campo, and K. Wei, 1996: Holocene environmental changes in Bangong Co basin (western Tibet). Part 4: Discussion and conclusions. *Palaeogeogr. Palaeoclimatol. Palaeoecol.,* **120,** 79–92.

Goswami, B. N., V. Krishnamurthy, and H. Annamalai, 1999: A broad-scale circulation index for the interannual variability of the Indian summer monsoon. *Quart. J. Roy. Meteor. Soc.,* **125,** 611–633.

——, M. S. Madhusoodanan, C. P. Neema, and D. Sengupta, 2006: A physical mechanism for North Atlantic SST influence on the Indian summer monsoon. *Geophys. Res. Lett.,* **33,** L02706, doi:10.1029/2005GL024803.

Gupta, A. K., D. M. Anderson, and J. T. Overpeck, 2003: Abrupt changes in the Asian southwest monsoon during the Holocene and their links to the North Atlantic Ocean. *Nature,* **421,** 354–357.

——, M. Das, S. C. Clemens, and B. Mukherjee, 2008: Benthic foraminiferal faunal and isotopic changes as recorded in Holocene sediments of the northwest Indian Ocean. *Paleoceanography,* **23,** PA2214, doi:10.1029/2007PA001546.

He, Y., W. H. Theakstone, Z. L. Zhang, D. A. Zhang, T. D. Yao, T. Chen, Y. P. Shen, and H. X. Pang, 2004: Asynchronous Holocene climatic change across China. *Quat. Res.,* **61,** 52–63.

Hendrickson, A. E., and P. O. White, 1964: Promax: A quick method for rotation to oblique simple structure. *Br. J. Stat. Psychol.,* **17,** 65–70.

Herzschuh, U., 2006: Palaeo-moisture evolution in monsoonal central Asia during the last 50,000 years. *Quat. Sci. Rev.,* **25,** 163–178.

Ho, C. H., J. Y. Lee, M. H. Ahn, and H. S. Lee, 2003: A sudden change in summer rainfall characteristics in Korea during the late 1970s. *Int. J. Climatol.,* **23,** 117–128.

Holmes, J. A., J. W. Zhang, F. H. Chen, and M. R. Qiang, 2007: Paleoclimatic implications of an 850-year oxygen-isotope record from the northern Tibetan Plateau. *Geophys. Res. Lett.,* **34,** L23403, doi:10.1029/2007GL032228.

Hu, C. Y., G. M. Henderson, J. H. Huang, S. Xie, Y. Sun, and K. R. Johnson, 2008: Quantification of Holocene Asian monsoon rainfall from spatially separated cave records. *Earth Planet. Sci. Lett.,* **266,** 221–232.

Huang, J. G., and Q. B. Zhang, 2007: Tree rings and climate for the last 680 years in Wulan area of northeastern Qinghai-Tibetan Plateau. *Climatic Change,* **80,** 369–377.

Huang, R. H., J. L. Chen, and G. Huang, 2007: Characteristics and variations of the East Asian monsoon system and its impacts on climate disasters in China. *Adv. Atmos. Sci.,* **24,** 993–1023.

Ishiwatari, R., K. Negishi, H. Yoshikawa, and S. Yamamoto, 2009: Glacial–interglacial productivity and environmental changes in Lake Biwa, Japan: A sediment core study of organic carbon, chlorins and biomarkers. *Org. Geochem.,* **40,** 520–530.

Iyengar, R. N., and P. Basak, 1994: Regionalization of Indian monsoon rainfall and long-term variability signals. *Int. J. Climatol.,* **14,** 1095–1114.

Kanamitsu, M., W. Ebisuzaki, J. Woollen, S.-K. Yang, J. J. Hnilo, M. Fiorino, and G. L. Potter, 2002: NCEP–DOE AMIP-II Reanalysis (R-2). *Bull. Amer. Meteor. Soc.,* **83,** 1631–1643.

Kansakar, S. R., D. M. Hannah, J. Gerrard, and G. Rees, 2004: Spatial pattern in the precipitation regime of Nepal. *Int. J. Climatol.,* **24,** 1645–1659.

Karl, T. R., A. J. Koscielny, and H. F. Diaz, 1982: Potential errors in the application of principal component (eigenvector) analysis to geophysical data. *J. Appl. Meteor.,* **21,** 1183–1186.

Kaspari, S., and Coauthors, 2007: Reduction in northward incursions of the South Asian monsoon since ~1400 AD inferred from a Mt. Everest ice core. *Geophys. Res. Lett.,* **34,** L16701, doi:10.1029/2007GL030440.

Kripalani, R. H., J. H. Oh, A. Kulkarni, S. S. Sabade, and H. S. Chaudhari, 2007: South Asian summer monsoon precipitation variability: Coupled climate model simulations and projections under IPCC AR4. *Theor. Appl. Climatol.,* **90,** 133–159.

Kudrass, H. R., A. Hofmann, H. Doose, K. Emeis, and H. Erlenkeuser, 2001: Modulation and amplification of climatic changes in the Northern Hemisphere by the Indian summer monsoon during the past 80 k.y. *Geology,* **29,** 63–66.

Kumar, K. K., B. Rajagopalan, and M. A. Cane, 1999: On the weakening relationship between the Indian monsoon and ENSO. *Science,* **284,** 2156–2159.

Kummerow, C., W. Barnes, T. Kozu, J. Shiue, and J. Simpson, 1998: The Tropical Rainfall Measuring Mission (TRMM) sensor package. *J. Atmos. Oceanic Technol.,* **15,** 809–817.

Lau, N.-C., and M. J. Nath, 2000: Impact of ENSO on the variability of the Asian–Australian monsoons as simulated in GCM experiments. *J. Climate,* **13,** 4287–4309.

——, and ——, 2003: Atmosphere–ocean variations in the Indo-Pacific sector during ENSO episodes. *J. Climate,* **16,** 3–20.

——, and ——, 2006: ENSO modulation of the interannual and intraseasonal variability of the East Asian monsoon—A model study. *J. Climate,* **19,** 4508–4530.

Lee, C. Y., and P. M. Liew, 2010: Late Quaternary vegetation and climate changes inferred from a pollen record of Dongyuan Lake in southern Taiwan. *Palaeogeogr. Palaeoclimatol. Palaeoecol.,* **287,** 58–66.

Lee, S. H., Y. Il Lee, H. Il Yoon, and K.-C. Yoo, 2008: East Asian monsoon variation and climate changes in Jeju Island, Korea, during the latest Pleistocene to early Holocene. *Quat. Res.,* **70,** 265–274.

Lee, S. M., J. G. Jhun, M. Kwon, and W. Kim, 2008: Change in the western North Pacific summer monsoon circulation due to the CO_2 increase in IPCC AR4 CGCMs. *Asia-Pac. J. Atmos. Sci.,* **44,** 351–368.

LeGrande, A. N., and G. A. Schmidt, 2009: Sources of Holocene variability of oxygen isotopes in paleoclimate archives. *Climate Past,* **5,** 441–455.

Li, J., and Q. Zeng, 2002: A unified monsoon index. *Geophys. Res. Lett.,* **29,** 1274, doi:10.1029/2001GL013874.

Liu, K. B., Z. J. Yao, and L. G. Thompson, 1998: A pollen record of Holocene climatic changes from the Dunde ice cap, Qinghai-Tibetan Plateau. *Geology,* **26,** 135–138.

Liu, T. S., and Z. L. Ding, 1998: Chinese loess and the paleomonsoon. *Annu. Rev. Earth Planet. Sci.,* **26,** 111–145.

Lu, H. L., Q. Q. Shao, J. Y. Liu, J. B. Wang, S. B. Chen, and Z. Q. Chen, 2008: Cluster analysis on summer precipitation field over Qinghai-Tibet Plateau from 1961 to 2004. *J. Geogr. Sci.,* **18,** 295–307.

Luckge, A., H. Doose-Rolinski, A. A. Khan, H. Schulz, and U. von Rad, 2001: Monsoonal variability in the northeastern Arabian Sea during the past 5000 years: Geochemical evidence from laminated sediments. *Palaeogeogr. Palaeoclimatol. Palaeoecol.,* **167,** 273–286.

Maxwell, A. L., 2001: Holocene monsoon changes inferred from lake sediment pollen and carbonate records, northeastern Cambodia. *Quat. Res.,* **56,** 390–400.

Meehl, G. A., 1997: The South Asian monsoon and the tropospheric biennial oscillation. *J. Climate,* **10,** 1921–1943.

——, and J. M. Arblaster, 2003: Mechanisms for projected future changes in South Asian monsoon precipitation. *Climate Dyn.,* **21,** 659–675.

——, and Coauthors, 2007: Global climate projections. *Climate Change 2007: The Physical Science Basis,* S. Solomon et al., Eds., Cambridge University Press, 747–845.

Mischke, S., M. Kramer, C. Zhang, H. Shang, U. Herzschuh, and J. Erzinger, 2008: Reduced early Holocene moisture availability in the Bayan Har Mountains, northeastern Tibetan Plateau, inferred from a multi-proxy lake record. *Palaeogeogr. Palaeoclimatol. Palaeoecol.,* **267,** 59–76.

Morinaga, H., and Coauthors, 1993: Oxygen-18 and carbon-13 records for the last 14,000 years from lacustrine carbonates of Siling-Co (Lake) in the Qinghai-Tibetan Plateau. *Geophys. Res. Lett.,* **20,** 2909–2912.

Morrill, C., J. T. Overpeck, and J. E. Cole, 2003: A synthesis of abrupt changes in the Asian summer monsoon since the last deglaciation. *Holocene,* **13,** 465–476.

——, ——, ——, K. B. Liu, C. M. Shen, and L. Y. Tang, 2006: Holocene variations in the Asian monsoon inferred from the

geochemistry of lake sediments in central Tibet. *Quat. Res.,* **65,** 232–243.

Mügler, I., and Coauthors, 2010: A multi-proxy approach to reconstruct hydrological changes and Holocene climate development of Nam Co, central Tibet. *J. Paleolimnol.,* **43,** 625–648.

North, G. R., T. L. Bell, R. F. Cahalan, and F. J. Moeng, 1982: Sampling errors in the estimation of empirical orthogonal functions. *Mon. Wea. Rev.,* **110,** 699–706.

Overland, J. E., and R. W. Preisendorfer, 1982: A significance test for principal components applied to a cyclone climatology. *Mon. Wea. Rev.,* **110,** 1–4.

Overpeck, J. T., and J. E. Cole, 2006: Abrupt change in earth's climate system. *Annu. Rev. Environ. Resour.,* **31,** 1–31.

——, D. Anderson, S. Trumbore, and W. Prell, 1996: The southwest Indian monsoon over the last 18 000 years. *Climate Dyn.,* **12,** 213–225.

Parthasarathy, B., A. A. Munot, and D. R. Kothawale, 1994: All-India monthly and seasonal rainfall series: 1871–1993. *Theor. Appl. Climatol.,* **49,** 217–224.

Prabhu, C. N., R. Shankar, K. Anupama, M. Taieb, R. Bonnefille, L. Vidal, and S. Prasad, 2004: A 200-ka pollen and oxygen-isotopic record from two sediment cores from the eastern Arabian Sea. *Palaeogeogr. Palaeoclimatol. Palaeoecol.,* **214,** 309–321.

Prasad, S., and Y. Enzel, 2006: Holocene paleoclimates of India. *Quat. Res.,* **66,** 442–453.

Quadrelli, R., and J. M. Wallace, 2004: A simplified linear framework for interpreting patterns of Northern Hemisphere wintertime climate variability. *J. Climate,* **17,** 3728–3744.

Rashid, H., B. P. Flower, R. Z. Poore, and T. M. Quinn, 2007: A ~25 ka Indian Ocean monsoon variability record from the Andaman Sea. *Quat. Sci. Rev.,* **26,** 2586–2597.

Rayner, N. A., D. E. Parker, E. B. Horton, C. K. Folland, L. V. Alexander, D. P. Rowell, E. C. Kent, and A. Kaplan, 2003: Global analyses of sea surface temperature, sea ice, and night marine air temperature since the late nineteenth century. *J. Geophys. Res.,* **108,** 4407, doi:10.1029/2002JD002670.

Richman, M. B., 1986: Rotation of principal components. *J. Climatol.,* **6,** 293–335.

Roy, P. D., W. Smykatz-Kloss, and R. Sinha, 2006: Late Holocene geochemical history inferred from Sambhar and Didwana playa sediments, Thar Desert, India: Comparison and synthesis. *Quat. Int.,* **144,** 84–98.

Ruddiman, W. F., 2006: What is the timing of orbital-scale monsoon changes? *Quat. Sci. Rev.,* **25,** 657–658.

Saji, N. H., B. N. Goswami, P. N. Vinayachandran, and T. Yamagata, 1999: A dipole mode in the tropical Indian Ocean. *Nature,* **401,** 360–363.

Sarkar, A., R. Ramesh, B. L. K. Somayajulu, R. Agnihotri, A. J. T. Jull, and G. S. Burr, 2000: High resolution Holocene monsoon record from the eastern Arabian Sea. *Earth Planet. Sci. Lett.,* **177,** 209–218.

Shankar, R., C. N. Prabhu, A. K. Warrier, G. T. V. Kumar, and B. Sekar, 2006: A multi-decadal rock magnetic record of monsoonal variations during the past 3,700 years from a tropical Indian tank. *J. Geol. Soc. India,* **68,** 447–459.

Shen, C. M., K. B. Liu, C. Morrill, J. T. Overpeck, J. Peng, and L. Y. Tang, 2008a: Ecotone shift and major droughts during the mid-late Holocene in the central Tibetan Plateau. *Ecology,* **89,** 1079–1088.

——, ——, and L. Y. Tang, 2008b: Numerical analysis of modern and fossil pollen data from the Tibetan Plateau. *Ann. Assoc. Amer. Geogr.,* **98,** 755–772.

Singh, K. K., and S. V. Singh, 1996: Space-time variation and regionalization of seasonal and monthly summer monsoon rainfall of the sub-Himalayan region and Gangetic plains of India. *Climate Res.,* **6,** 251–262.

Sinha, A., K. G. Cannariato, L. D. Stott, H. Cheng, R. L. Edwards, M. G. Yadava, R. Ramesh, and I. B. Singh, 2007: A 900-year (600 to 1500 A. D.) record of the Indian summer monsoon precipitation from the core monsoon zone of India. *Geophys. Res. Lett.,* **34,** L16707, doi:10.1029/2007GL030431.

Sirocko, F., M. Sarnthein, H. Erlenkeuser, H. Lange, M. Arnold, and J. C. Duplessy, 1993: Century-scale events in monsoonal climate over the past 24,000 years. *Nature,* **364,** 322–324.

Staubwasser, M., 2006: An overview of Holocene South Asian monsoon records—Monsoon domains and regional contrasts. *J. Geol. Soc. India,* **68,** 433–446.

——, F. Sirocko, P. M. Grootes, and M. Segl, 2003: Climate change at the 4.2 ka BP termination of the Indus valley civilization and Holocene South Asian monsoon variability. *Geophys. Res. Lett.,* **30,** 1425, doi:10.1029/2002GL016822.

Sun, D. H., M. K. Gagan, H. Cheng, H. Scott-Gagan, C. A. Dykoski, R. L. Edwards, and R. X. Sua, 2005: Seasonal and interannual variability of the mid-Holocene East Asian monsoon in coral $\delta^{18}O$ records from the South China Sea. *Earth Planet. Sci. Lett.,* **237,** 69–84.

Tang, L. Y., and Coauthors, 2009: Pollen-inferred vegetation and environmental changes in the central Tibetan Plateau since 8200 yr BP. *Sci. China,* **52D,** 1104–1114.

Thompson, L. G., and Coauthors, 1997: Tropical climate instability: The last glacial cycle from a Qinghai-Tibetan ice core. *Science,* **276,** 1821–1825.

——, T. Yao, E. Mosley-Thompson, M. E. Davis, K. A. Henderson, and P. N. Lin, 2000: A high-resolution millennial record of the South Asian monsoon from Himalayan ice cores. *Science,* **289,** 1916–1919.

Tian, L., V. Masson-Delmotte, M. Stievenard, T. Yao, and J. Jouzel, 2001: Tibetan Plateau summer monsoon northward extent revealed by measurements of water stable isotopes. *J. Geophys. Res.,* **106,** 28 081–28 088.

Trenberth, K. E., D. P. Stepaniak, and J. M. Caron, 2000: The global monsoon as seen through the divergent atmospheric circulation. *J. Climate,* **13,** 3969–3993.

Treydte, K. S., G. H. Schleser, G. Helle, D. C. Frank, M. Winiger, G. H. Haug, and J. Esper, 2006: The twentieth century was the wettest period in northern Pakistan over the past millennium. *Nature,* **440,** 1179–1182.

Turner, A. G., P. A. Inness, and J. M. Slingo, 2007: The effect of doubled CO_2 and model basic state biases on the monsoon-ENSO system. I: Mean response and interannual variability. *Quart. J. Roy. Meteor. Soc.,* **133,** 1143–1157.

Van Campo, E., 1986: Monsoon fluctuations in two 20,000-yr BP oxygen-isotope/pollen records off southwest India. *Quat. Res.,* **26,** 376–388.

Wang, B., and Z. Fan, 1999: Choice of South Asian summer monsoon indices. *Bull. Amer. Meteor. Soc.,* **80,** 629–638.

—— and LinHo, 2002: Rainy season of the Asian–Pacific summer monsoon. *J. Climate,* **15,** 386–398.

——, R. Wu, and X. Fu, 2000: Pacific–East Asian teleconnection: How does ENSO affect East Asian climate? *J. Climate,* **13,** 1517–1536.

——, ——, and K.-M. Lau, 2001: Interannual variability of the Asian summer monsoon: Contrasts between the Indian and the western North Pacific–East Asian monsoons. *J. Climate,* **14,** 4073–4090.

——, S. C. Clemens, and P. Liu, 2003: Contrasting the Indian and East Asian monsoons: Implications on geologic timescales. *Mar. Geol.,* **201,** 5–21.

——, Z. W. Wu, J. P. Li, J. Liu, C. P. Chang, Y. H. Ding, and G. X. Wu, 2008: How to measure the strength of the East Asian summer monsoon. *J. Climate,* **21,** 4449–4463.

Wang, H., H. Liu, J. Zhu, and Y. Yin, 2010: Holocene environmental changes as recorded by mineral magnetism of sediments from Anguli-nuur Lake, southeastern Inner Mongolia Plateau, China. *Palaeogeogr. Palaeoclimatol. Palaeoecol.,* **285,** 30–49.

Wang, L., and Coauthors, 1999: East Asian monsoon climate during the late Pleistocene: High-resolution sediment records from the South China Sea. *Mar. Geol.,* **156,** 245–284.

Wang, R. L., S. C. Scarpitta, S. C. Zhang, and M. P. Zheng, 2002: Later Pleistocene/Holocene climate conditions of Qinghai-Xizhang Plateau (Tibet) based on carbon and oxygen stable isotopes of Zabuye Lake sediments. *Earth Planet. Sci. Lett.,* **203,** 461–477.

Wang, X. C., Q. B. Zhang, K. P. Ma, and S. C. Xiao, 2008: A tree-ring record of 500-year dry-wet changes in northern Tibet, China. *Holocene,* **18,** 579–588.

Wang, Y. J., H. Cheng, R. L. Edwards, Z. S. An, J. Y. Wu, C. C. Shen, and J. A. Dorale, 2001: A high-resolution absolute-dated late Pleistocene monsoon record from Hulu Cave, China. *Science,* **294,** 2345–2348.

——, and Coauthors, 2005: The Holocene Asian monsoon: Links to solar changes and North Atlantic climate. *Science,* **308,** 854–857.

——, and Coauthors, 2008: Millennial- and orbital-scale changes in the East Asian monsoon over the past 224,000 years. *Nature*, **451,** 1090–1093.

Webster, P. J., 2006: The coupled monsoon system. *The Asian Monsoon,* B. Wang, Ed., 3–66.

——, and S. Yang, 1992: Monsoon and ENSO: Selectively interactive systems. *Quart. J. Roy. Meteor. Soc.,* **118,** 877–926.

——, V. O. Magaña, T. N. Palmer, J. Shukla, R. A. Tomas, M. Yanai, and T. Yasunari, 1998: Monsoons: Processes, predictability, and the prospects for prediction. *J. Geophys. Res.*, **103C,** 14 451–14 510.

Wei, K., and F. Gasse, 1999: Oxygen isotopes in lacustrine carbonates of west China revisited: Implications for post glacial changes in summer monsoon circulation. *Quat. Sci. Rev.,* **18,** 1315–1334.

Wei, K. Y., T. C. Chiu, and Y. G. Chen, 2003: Toward establishing a maritime proxy record of the East Asian summer monsoons for the Late Quaternary. *Mar. Geol.,* **201,** 67–79.

White, D., M. Richman, and B. Yarnal, 1991: Climate regionalization and rotation of principal components. *Int. J. Climatol.,* **11,** 1–25.

Winkler, M. G., and P. K. Wang, 1993: The late-Quaternary vegetation and climate of China. *Global Climates since the Last Glacial Maximum,* H. E. Wright et al., Eds., University of Minnesota Press, 221–264.

Wünnemann, B., S. Mischke, and F. H. Chen, 2006: A Holocene sedimentary record from Bosten Lake, China. *Palaeogeogr. Palaeoclimatol. Palaeoecol.,* **234,** 223–238.

Xiao, J. L., J. T. Wu, B. Si, W. D. Liang, T. Nakamura, B. L. Liu, and Y. Inouchi, 2006: Holocene climate changes in the monsoon/arid transition reflected by carbon concentration in Daihai Lake of Inner Mongolia. *Holocene,* **16,** 551–560.

Xie, P. P., and P. A. Arkin, 1997: Global precipitation: A 17-year monthly analysis based on gauge observations, satellite estimates, and numerical model outputs. *Bull. Amer. Meteor. Soc.,* **78,** 2539–2558.

Yadava, M. G., and R. Ramesh, 2006: Stable oxygen and carbon isotope variations as monsoon proxies: A comparative study of speleothems from four different locations in India. *J. Geol. Soc. India,* **68,** 461–475.

Yang, S., and K. M. Lau, 2006: Interannual variability of the Asian Monsoon. *The Asian Monsoon,* B. Wang, Ed., Springer-Verlag, 259–293.

Yuan, D., and Coauthors, 2004: Timing, duration, and transitions of the last interglacial Asian monsoon. *Science,* **304,** 575–578.

Zhang, P., and Coauthors, 2008: A test of climate, sun, and culture relationships from an 1810-year Chinese cave record. *Science,* **322,** 940–942.

Zhang, R., and T. L. Delworth, 2006: Impact of Atlantic multidecadal oscillations on India/Sahel rainfall and Atlantic hurricanes. *Geophys. Res. Lett.,* **33,** L17712, doi:10.1029/2006GL026267.

Zhang, S. P., and B. Wang, 2008: Global summer monsoon rainy seasons. *Int. J. Climatol.,* **28,** 1563–1578.

Zhou, T. J., and Coauthors, 2009: The CLIVAR C20C project: Which components of the Asian–Australian monsoon circulation variations are forced and reproducible? *Climate Dyn.,* **33,** 1051–1068.

Zonneveld, K. A. F., G. Ganssen, S. Troelstra, G. J. M. Versteegh, and H. Visscher, 1997: Mechanisms forcing abrupt fluctuations of the Indian Ocean summer monsoon during the last deglaciation. *Quat. Sci. Rev.,* **16,** 187–201.

CORRIGENDUM

JESSICA L. CONROY

Department of Geosciences, The University of Arizona, Tucson, Arizona

JONATHAN T. OVERPECK

Department of Geosciences, Department of Atmospheric Sciences, and Institute of the Environment, The University of Arizona, Tucson, Arizona

(Manuscript received 23 August 2011, in final form 7 September 2011)

Two figures in Conroy and Overpeck (2011) were not reproduced correctly in the final published version of the paper. These two figures (Fig. 2 and Fig. 4) are presented here as they were meant to be published.

The staff of the *Journal of Climate* regrets any inconvenience these errors may have caused.

REFERENCE

Conroy, J. L., and J. T. Overpeck, 2011: Regionalization of present-day precipitation in the greater monsoon region of Asia. *J. Climate,* **24,** 4073–4095.

DOI: 10.1175/JCLI-D-11-00485.1

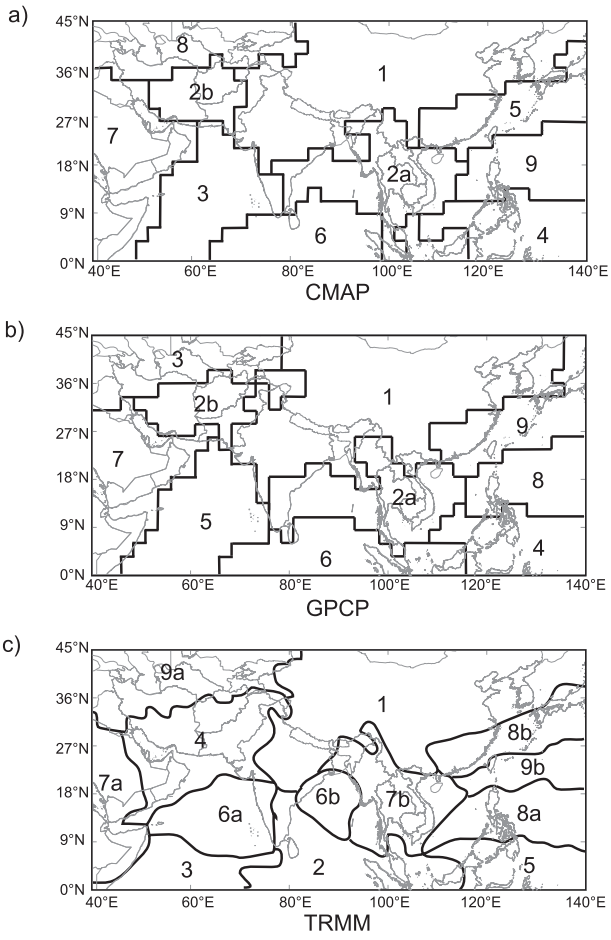

FIG. 2. Regions delimited by maximum loading values for the (a) CMAP, (b) GPCP, and (c) TRMM datasets.

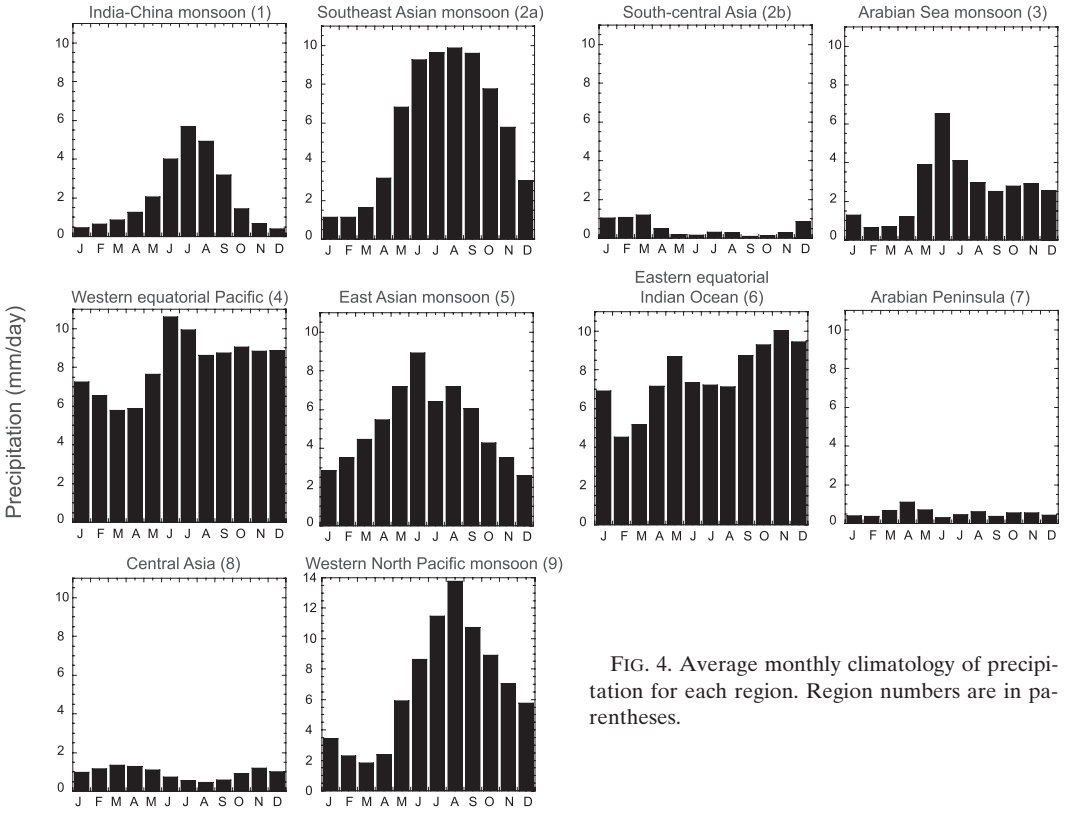

FIG. 4. Average monthly climatology of precipitation for each region. Region numbers are in parentheses.